New Insights on the Distribution of Interlayer Water in Bi-Hydrated Smectite from X-ray Diffraction Profile Modeling of 00l Reflections — Source link

Eric Ferrage, Bruno Lanson, Natalie Malikova, A. Plançon ...+2 more authors

Institutions: Centre national de la recherche scientifique, Russian Academy of Sciences

Related papers:

- Investigation of smectite hydration properties by modeling experimental X-ray diffraction patterns: Part I. Montmorillonite hydration properties

- Investigation of dioctahedral smectite hydration properties by modeling of X-ray diffraction profiles: Influence of layer charge and charge location

- Mechanism of adsorption and desorption of water vapor by homoionic montmorillonite: 3. The Mg2+, Ca2+, Sr2+ and Ba2+ exchanged forms

- Hydration Properties and Interlayer Organization of Water and Ions in Synthetic Na-Smectite with Tetrahedral Layer Charge. Part 1. Results from X-ray Diffraction Profile Modeling

- Mechanism of Adsorption and Desorption of Water Vapor by Homoionic Montmorillonites: 2. The Li+ Na+, K+, Rb+ and Cs+-Exchanged Forms

New insights on the distribution of interlayer water in bi-hydrated smectite from X-ray diffraction profile modeling 00l reflections

Eric Ferrage, Bruno Lanson, Natalie Malikova, Alain Plançon, Boris.A. Sakharov, Victor.A. Drits

1   New insights on the distribution of interlayer water in bi-hydrated smectite from

2   X-ray diffraction profile modeling of 00ℓ reflections

3

4

5

6

7   Eric Ferrage[1,2], Bruno Lanson[1,*], Natalie Malikova[2,3], Alain Plançon[4], Boris A. Sakharov[1,5],

8   and Victor A. Drits[1,5]

9

10   [1] Environmental Geochemistry Group, LGIT – Maison des Géosciences, Joseph Fourier

11   University – CNRS, BP53, F-38041 Grenoble cedex 9, France

12   [2] ANDRA, Parc de la Croix Blanche, 1-7 rue Jean Monnet, F-92298 Châtenay-Malabry

13   cedex, France

14   [3] Laboratory Liquides Ioniques & Interfaces Chargées, Paris 06 University, Case

15   Courrier 51, 4 Pl. Jussieu, F-75252 Paris; France

16   [4] Crystallography Laboratory, ISTO, University of Orléans - CNRS, F-45067 Orléans

17   Cedex 2, France.

18   [5] Geological Institute, Russian Academy of Sciences, 7 Pyzhevsky street, 109017

19   Moscow, Russia

20

21   * Author to whom correspondence should be addressed.

22   e-mail : Bruno.Lanson@obs.ujf-grenoble.fr

23   **Abstract**

24

25   The interlayer configuration proposed by Moore and Reynolds and commonly used to

26   reproduce the 00ℓ reflections of bi-hydrated smectite is shown to be inconsistent with

27   experimental X-ray diffraction data.[1] The alternative configuration of interlayer species with

28   cations located in the mid-plane of the interlayer and one sheet of H_2O molecules on each side

29   of this plane is also shown to imperfectly describe the actual structure of bi-hydrated

30   smectites. Specifically, the thermal fluctuation of atomic positions (Debye-Waller factor) used

31   to describe the positional disorder of interlayer H_2O molecules has to be increased to

32   unrealistic values to satisfactorily reproduce experimental X-ray diffraction data when using

33   this model. A new configuration is thus proposed for the interlayer structure of bi-hydrated

34   smectite. Cations are located in the mid-plane of the interlayer whereas H_2O molecules are

35   scattered about two main positions according to Gaussian-shaped distributions. This

36   configuration allows reproducing all 00ℓ reflections with a high precision, with only one new

37   variable parameter (width of the Gaussian function). The proposed configuration is consistent

38   with those derived from Monte-Carlo calculations and allows matching more closely the

39   amount of interlayer water that can be determined independently from water vapor

40   adsorption/desorption isotherm experiments. In addition, the proposed configuration of

41   interlayer species appears valid for both dioctahedral and trioctahedral smectites exhibiting

42   octahedral and tetrahedral substitutions, respectively, thus not allowing to differentiate these

43   expandable 2:1 phyllosilicates from their respective interlayer configuration.

Introduction

46   Smectite is a 2:1 phyllosilicate whose layer structure consists of an octahedral sheet

47   sandwiched in-between two siliceous tetrahedral sheets. Isomorphic substitutions in either

48   tetrahedral or octahedral sites induce a permanent negative layer charge, which is

49   compensated for by the presence of hydrated cations in the interlayer. The observation of 00ℓ

50   basal reflections on X-ray diffraction (XRD) patterns has shown that with increasing relative

51   humidity smectite expands stepwise, the different steps corresponding to the intercalation of

52   0, 1, 2 or 3 sheets of H_2O molecules in the interlayer.[2-6] From these pioneer studies, it is now

53   commonly accepted that the expandability of 2:1 phyllosilicates is controlled by factors such

54   as the nature of interlayer cations, and the layer charge and its location (octahedral vs.

55   tetrahedral). These general observations have led to different models in which crystalline

56   swelling is controlled by the balance between the repulsive forces between neighboring 2:1

57   layers and the attractive forces between hydrated interlayer cations and the negatively-charged

58   surface of siloxane sheets.[6-11]

59   The development of XRD modeling techniques allowed investigating structures in

60   which different hydration states coexist thus improving these early observations.[12-17] Ferrage

61   et al. used such a modeling approach to characterize the hydration of several montmorillonite

62   and beidellite samples and observed that the nature of the interlayer cation, and in particular

63   its affinity for water, influences the layer thickness of bi-hydrated and monohydrated

64   layers.[18,19] They also confirmed that the relative proportions of the different layer types,

65   which correspond to the different hydration states, depend on both the amount and the

66   location of smectite layer charge. In addition, these authors showed that XRD peak profiles

67   and position can be satisfactorily reproduced, especially over the low-angle region (~5-12°2θ

68   Cu Kα), only if hydration heterogeneity is taken into account. They were thus able to refine

69   the structure of smectite and in particular to investigate atomic positions of interlayer species.

70   In particular, they showed that the atomic positions reported by Moore and Reynolds for H_2O

71   molecules in bi-hydrated layers induce a dramatic misfit over the medium- to high-angle

72   region (12-50°2θ Cu Kα) by strongly modifying the intensity ratio between the different 00ℓ

73   reflections.[1,18]

74   The present article thus aims at refining further the structure of interlayer H_2O in bi-

75   hydrated smectites from the fit of experimental XRD patterns. The proposed structure is

76   compared with the positional distribution commonly derived from Monte-Carlo simulations,

77   whereas the adjusted amounts of interlayer water are compared with those determined

78   experimentally from water vapor adsorption-desorption experiments.

79

80   **Background**

81

82   **Smectite hydration heterogeneity as seen by XRD profile modeling.** In agreement

83   with the stepwise evolution of the d_{001} basal spacing on XRD patterns, the hydration state of

84   smectite has been described using three layer types exhibiting different layer thickness

85   corresponding to the common hydration states reported for montmorillonite in non-saturated

86   conditions. Dehydrated layers (0W – Layer thickness ~9.6-10.1 Å), mono-hydrated layers

87   (1W – Layer thickness ~12.3-12.7 Å), and bi-hydrated layers (2W – Layer thickness ~15.1-

88   15.8 Å) have thus been defined. In the first two layer types, interlayer cations are located in

89   the mid-plane of the interlayer, together with H_2O molecules for 1W layers. For 2W layers,

90   interlayer cations are also commonly assumed to be located in the mid-plane of the

91   interlayer.[1] In addition, it is usually assumed that two planes of H_2O molecules, each bearing

92   0.69 H_2O per $O_{20}(OH)_4$, are located at 0.35 and 1.06 Å from the cation along the c* axis

93   (Debye-Waller parameter B_{wat} ~2 Å^2 for these two planes), whereas a third denser plane (1.20

94　H$_2$O per O$_{20}$(OH)$_4$) is located further from the central interlayer cation at 1.20 Å along the c*

95　axis (B$_{wat}$ = 11 Å^2).[1] The pattern calculated for the Ca-saturated reference SWy-1

96　montmorillonite (Ca-SWy-1) assuming a homogeneous 2W hydration state and the above

97　configuration for interlayer species is compared on Figure 1a to the experimental pattern

98　recorded at 80% RH. With these usual hypotheses, the calculated pattern fits most of the

99　experimental pattern features but significant discrepancies can be observed over the medium-

100　to the high-angle region in spite of the low intensity diffracted. In particular, the position of

101　the 005 reflection and the low-angle "tail" of the 002 reflection are not well reproduced

102　(Figure 1a). Ferrage et al. challenged this usual configuration of interlayer species, and

103　proposed an alternative configuration that includes a unique plane of H$_2$O molecules located

104　at 1.20 Å, along the c* axis, on either side of the central interlayer cation (2WS

105　configuration).[18] The use of this 2WS configuration helps reducing the discrepancies observed

106　for the 003-005 reflections. In particular, this configuration allows decreasing the relative

107　intensity of the 003 and 004 reflections whereas the intensity of the 005 one is increased

108　(Figure 1b). However, in the high-angle region the intensity ratio between the 007 and 008

109　reflections measured on the calculated pattern is inconsistent with that determined

110　experimentally, although the intensity of the 008 reflection is correctly reproduced.

111　　　Ferrage et al. also demonstrated that the common hypothesis of a homogeneous

112　hydration state for smectite is not consistent with the likely existence in smectite of structural

113　heterogeneities affecting the layer charge distribution (from one interlayer to the other or

114　within a given interlayer) and/or location (octahedral vs. tetrahedral).[18] In turn these

115　heterogeneities lead to the coexistence of different layer types in a single structure. Such

116　hydration heterogeneity has been evidenced from the profile modeling of XRD patterns

117　recorded on hydrated smectites.[12-17] Ferrage et al. have shown that this heterogeneity is

118　systematically observed whatever the interlayer cation, the relative humidity (RH), and the

119 amount and location of the layer charge deficit.[18,19] It is thus essential to account for the

120 hydration heterogeneity to satisfactorily reproduce the experimental positions and profiles of

121 reflections.

122   Ferrage et al. have shown indeed that accounting for smectite hydration heterogeneity

123 allows fitting better the profiles of all experimental 00ℓ reflections.[18,19] In particular

124 heterogeneous samples were modeled by combining the contributions of several structures,

125 each containing either one (periodic structure) or different layer types (mixed-layer structure –

126 MLS) randomly interstratified (R=0).[18-20] These different contributions should be seen as a

127 simplified way to describe the actual hydration heterogeneity of the sample under

128 investigation, with the different layer types not being distributed at random in the different

129 crystallites. However, the coexistence of these contributions does not imply the actual

130 presence of populations of particles in the sample, as their relative proportions may vary as a

131 function of RH for example.[18] To account for the heterogeneous distribution of the different

132 layer types within smectite crystallites, layers exhibiting the same hydration state that are

133 present in the different MLSs must have identical properties as they may be accounted for in

134 one or the other structure depending on the RH. In particular for a given XRD pattern, each

135 layer type must possess a constant crystal-chemistry in the different MLSs. It was possible to

136 reproduce the profile of all experimental 00ℓ reflections of the experimental XRD pattern

137 recorded on Ca-SWy-1 at 80% RH by considering two MLSs (Figure 1c) and the 2WS

138 configuration for interlayer water.[18] Specifically, the position of the 005 reflection, the low-

139 angle shoulder of the 002 reflection and the "tails" of the 001 reflection are satisfactorily

140 reproduced by taking hydration heterogeneity into account. Accounting for hydration

141 heterogeneity also helps reproducing the relative intensity of higher-angle reflections (002,

142 003, 004, and 005 for example) but significant discrepancies that could result from an

143 incorrect structure model for interlayer water are still visible for high-angle reflections (Figure

144 1c). Specifically, the 006, 007 and 008 reflections are not satisfactorily reproduced, as for

145 example the intensity ratio between the 007 and 008 reflections measured on experimental

146 and calculated patterns are inconsistent. These discrepancies are reduced by increasing the

147 Debye-Waller factor of H_2O molecules (B_{wat}) from 2 to 11 $Å^2$ for this 2WS configuration of

148 interlayer H_2O molecules (Figure 1d).[18] However, such high values of the Debye-Waller

149 factor are not sufficient to conceal the disagreement for the intensity ratio between 007 and

150 008 reflections, and thermal atomic fluctuations most likely do not adequately describe the

151 positional distribution of H_2O molecules in 2W smectite layers, and additional hypotheses

152 have to be sought.

153   **Interlayer configuration of 2W smectite layers as seen by Monte-Carlo**

154 **simulations**. In the above calculations, H_2O molecules are distributed in discrete planes, and

155 the positional distribution of H_2O molecules results only from their thermal motion. However,

156 this simplified description of the smectite interlayer structure does not allow fitting the

157 experimental XRD data (Figures 1c, 1d) most likely because the description of H_2O molecule

158 positional disorder is incomplete. A more complete (realistic ?) description of the interlayer

159 structure may be obtained from Monte-Carlo (MC) simulations which allow taking into

160 account all interactions among interlayer species, as well as between these species and the 2:1

161 layer.[21] It is in particular possible to account for the hydration variability of interlayer cation

162 which can form either inner-sphere or outer-sphere complexes with the 2:1 layer surface,

163 leading to the existence or to the lack, respectively, of direct interactions with O atoms from

164 the layer surface. In the latter case, these interactions are screened by H_2O molecules from the

165 cation hydration sphere. It has been shown that, as compared to other monovalent cations, K^+

166 cations tend to form inner-sphere complexes in montmorillonite interlayers and that these

167 cations remain partially bound to the 2:1 clay surface even in the 2W state.[22,23] On the

168 contrary, Li^+ and Na^+ cations in 2W smectites are located in the mid-plane of the interlayer.[23-

169   The location of the layer charge deficit has also been shown to influence the hydration of

170   interlayer Na^+ cations, the formation of inner-sphere complexes being favored by tetrahedral

171   substitutions.[26] On the other hand, a majority of interlayer Na^+ cations is located in the mid-

172   plane of the interlayer for octahedrally substituted 2W smectites.[23,24] A similar influence of

173   the charge location was reported for K- and Li-saturated 2W smectites.[22,25] In contrast,

174   whatever the charge location Mg^{2+} cations are systematically octahedrally coordinated in 2W

175   smectites and located in the mid-plane of the interlayer.[27,28] In any case, MC simulations most

176   often indicate that H_2O molecules do not form a discrete plane but rather show that they are

177   distributed about a "most probable" position. In addition, the mixed charge location common

178   in smectite layers, and more especially in those of natural samples, can lead to the coexistence

179   in a single smectite interlayer of different complexes, thus broadening the water distribution

180   profile by perturbing the hydrogen bond network and the orientation of the water dipole.[29]

181   Even though MC simulations do not commonly account for smectite hydration heterogeneity,

182   which is best revealed by XRD analysis, such a description of H_2O molecules positional

183   disorder could be the missing link toward a better structure determination of H_2O

184   configuration in 2W smectite layers.

185

186   **Materials and Methods**

187

188   **Experimental**. Samples investigated in the present work include two reference low-

189   charge montmorillonites (SWy-1 and SWy-2) available from the Source Clays Repository

190   (http://www.agry.purdue.edu/cjohnston/sourceclays/index.html) and two synthetic saponite

191   samples. The latter samples were selected because of their contrasting layer charges (0.8 and

192   1.4 per $O_{20}(OH)_4$).[30,31] The size fractionation of all samples, and their homoionic saturation

193   were performed as described by Ferrage et al.[18] For all samples, oriented slides were prepared

194   by drying at room temperature a clay slurry pipetted onto a glass slide. XRD patterns were

195   then recorded using a Bruker D5000 diffractometer equipped with a Kevex Si(Li) solid-state

196   detector, an Ansyco rh-plus 2250 humidity control device coupled to an Anton Paar TTK450

197   chamber. Usual scanning parameters were $0.04°2\theta$ as step size and 6s as counting time per

198   step over the $2\text{-}50°2\theta$ Cu Kα angular range. The divergence slit, the two Soller slits, the

199   antiscatter and resolution slits were $0.5°$, $2.3°$, $2.3°$, $0.5°$ and $0.06°$, respectively. Data

200   collection conditions (60 and 80% RH for Sr-saturated samples, 40 and 80% RH for Ca-

201   saturated samples, and 80 or 90% RH for Na-saturated samples) were selected because of the

202   high amount of 2W layers (>90%) present in these conditions.[18]

203   **Simulation of X-ray diffraction data**. The algorithms developed initially by Drits

204   and coworkers were used to fit experimental XRD profiles over the $2\text{–}50°2\theta$ CuKα range

205   using a trial-and-error approach.[32-34] Instrumental and experimental factors such as horizontal

206   and vertical beam divergences, goniometer radius, length and thickness of the oriented slides

207   were measured and introduced without further adjustment. The mass absorption coefficient

208   (μ^*) was set to 45 cm^{2}g^{-1}, as recommended by Moore and Reynolds,[1] whereas the parameter

209   characterizing the preferred orientation of the particles in the sample (σ^*) was considered as a

210   variable parameter. Additional variable parameters include the coherent scattering domain

211   size (CSDS) along the c* axis which was characterized by a maximum CSDS value, set to 45

212   layers, and by a variable mean CSDS value (N).[35] In addition, because of the weak bonds

213   between adjacent smectite layers, layer thickness was allowed to deviate from the average d_{001}

214   value. This cumulative deviation from periodicity, which is described as a "disorder of the

215   second type",[36,37] is accounted for by introducing a variance parameter σ_z.[18] z-coordinates of

216   all atoms building up the 2:1 layer framework as well as those present in the interlayer of 0W

217   and 1W layers were set as proposed by Moore and Reynolds.[1] The interlayer structure of 2W

218   layers has been refined to account for all features of experimental XRD patterns recorded on

219   2W-dominated samples. In particular, a double Gaussian distribution of H_2O molecules along

220   the c* axis (2WG) was assumed. This 2WG model accounts both for the presence of a unique

221   plane of H_2O molecules on either side of the mid-plane (Figures 1c, 1d) and for the positional

222   distribution of H_2O molecules derived from MC simulations incomplete. The 2WG

223   distributions considered in the present study are symmetrical relative to the interlayer mid-

224   plane. They are characterized by the distance (Δd) between this mid-plane, where interlayer

225   cations are supposed to be located, and the position of the maximum density of the Gaussian

226   distribution. In addition, the total amount of interlayer H_2O molecules was refined together

227   with the full width at half maximum intensity (FWHM) parameter of the Gaussian

228   distribution. In the resulting structure model, H_2O molecules were introduced using a 0.05 Å

229   step along the c* axis, with a B_{wat} factor equal to zero, as thermal motion is taken into account

230   in MC calculations.

231   Two parameters were used to assess the overall goodness of fit. The unweighted R_p

232   parameter was considered because this parameter is mainly influenced by the most intense

233   diffraction maxima such as the 001 reflection which contains essential information on the

234   proportions of the different layer types and on their respective layer thickness values. The R_{wp}

235   parameter was also used to better account for the overall fit quality, especially in the high-

236   angle regions.[38] Accessory quartz reflections were omitted for the calculation of these

237   parameters. On their low-angle side, calculated XRD patterns are limited to ~5°2θ CuKα

238   because significant discrepancies, possibly resulting from an incorrect description of

239   crystalline defects not challenging the results described in the present study,[18] are observed

240   over the low-angle region.[39]

241   **Monte-Carlo simulations**. Monte-Carlo simulations in the NVT ensemble were used

242   to obtain a detailed spatial distribution of the different species within smectite interlayers. The

243   model   montmorillonite-type   smectite   used   in   the   simulations   has   a

244    $Na_{0.75}(Si_8)(Al_{3.25}Mg_{0.75})O_{20}(OH)_4$ structural formula and exhibits substitutions only in the

245   octahedral sheet. The simulation box includes two 2:1 layers, each consisting of 8 unit cells

246   (total area: 20.72 Å × 17.94 Å, thickness of the 2:1 layer: 6.54 Å). The total negative charge

247   of the 2:1 layers was thus compensated for by 6 Na^+ cations in the interlayer. The interlayer

248   shift between adjacent 2:1 layers was set to different arbitrary values for the two interlayers

249   considered and not allowed to vary during the calculation. For the typical layer thickness

250   value (15.52 Å) determined for Na-montmorillonite by XRD profile modeling, the water

251   content was estimated from the results of previous MC simulations performed with the NPT

252   ensemble. Series of such simulations allows the determination of layer thickness as a function

253   of water content, at constant pressure and temperature,[40] and the water content was found to

254   be 9.5 H_2O molecules per $O_{20}(OH)_4$. The resulting distributions of H_2O molecules within 2W

255   smectite interlayers were collected over 5 million MC steps, normalized and made symmetric

256   with respect to the mid-plane of the interlayer. The 2:1 layers were considered as rigid, and

257   modeled with the rigid SPC/E model (O-H bond 1.0 Å, angle H-O-H 109.47°, charges

258   -0.848 e^- and +0.424 e^- for oxygen and hydrogen atoms, respectively). Applied interaction

259   potentials were the Lennard-Jones 6-12 and Coulombic potentials. Each atom in the

260   simulation cell was thus characterized by two Van der Waals parameters and by its charge.

261   Additional details on the MC simulations can be found elsewhere.[25,41-43] Density profiles

262   determined from MC calculations for interlayer sodium and H_2O molecules were introduced

263   in the XRD profile calculation using a 0.075 Å step.

264

265   **Results**

266

267   **Influence of the Gaussian distribution profile on the relative intensity of 00ℓ**

268   **reflections**. Figure 2 illustrates the influence of the different parameters used to describe the

269   Gaussian distribution of H_2O molecules, that is the total amount of H_2O molecules (nH_2O),

270   Δd, and FWHM, on the relative intensity of 00ℓ reflections. Calculations were performed

271   assuming a periodic Ca-SWy-1 2W structure (layer thickness = 15.2 Å), and calculated

272   intensities were systematically normalized to that of the 001 reflection. By increasing the total

273   amount of H_2O molecules the intensity of the 002, 003, 005 reflections greatly increases, that

274   of the 008 reflection also increases but to a lower extent whereas 004, 006 and 007 reflections

275   are essentially unaffected (Figure 2). As its influence on 007 and 008 reflection intensity is

276   limited, the nH_2O parameter will not affect significantly the intensity ratio between these two

277   reflections which is a common and critical discrepancy between experimental and calculated

278   profiles (Figures 1a-d). On the contrary, the 008:007 intensity ratio is strongly affected by the

279   FWHM of the Gaussian distribution, this ratio being minimum for a Dirac distribution and

280   increasing with the FWHM of the distribution. The 007 reflection is actually more intense

281   than the 008 one for FWHM values larger than ~1.3 Å (Figure 2). In addition this parameter

282   may be strongly constrained from its major influence on the intensity ratio between two

283   intense reflections (003 and 005 reflections) which can be reversed by increasing the width of

284   the Gaussian distribution of H_2O molecules. However, the 003:005 ratio is also affected by

285   the Δd parameter which also affects the 008:007 intensity ratio, both ratios increasing with

286   increasing Δd values. By increasing either the Δd parameter or the FWHM, the intensity of

287   the 002 reflection is systematically decreased, whereas that of the 004 reflection is increased

288   or decreased, respectively. The intensity calculated for the 006 reflection is low whatever the

289   values used for these two parameters.

290   **Modeling of XRD patterns**. For all XRD patterns recorded on smectite samples,

291   calculations were performed using three different configurations of H_2O molecules in the

292   interlayers of 2W layers: (i) a 2WS configuration with two planes of H_2O molecules

293   characterized by a B_{wat} factor of 2 Å^2 and a Δd parameter of 1.2 Å,[18] (ii) a similar 2WS

294 configuration with a larger Debye-Waller factor (B_{wat} = 11 Å^2), and (iii) a configuration with

295 H_2O molecules distributed according to the 2WG configuration. Optimum parameters used to

296 characterize smectite hydration heterogeneity, that is the relative proportions of the different

297 MLSs coexisting in the sample and their compositions (relative proportions of 2W, 1W, and

298 0W layers) are reported in Table 1 together with the layer thickness values for the different

299 layer types, N, σ^*, σ_z and the water content in 1W layers. For 2W layers, the water content,

300 the Δd parameter, and the FWHM of the Gaussian distribution are reported in Table 2 for the

301 different configurations of interlayer H_2O molecules.

302 *Ca-saturated montmorillonite*. For sample Ca-SWy-1 at 80% RH, the calculations

303 performed for 2WS configurations of H_2O molecules (Δd = 1.2 Å) and B_{wat} factors of 2 and

304 11 Å^2 have been described above (Figures 1c, 1d). The 2WS configuration provides a

305 satisfactory fit to experimental patterns for 00ℓ reflections with ℓ<6. However, this model

306 does not allow concealing the discrepancy observed over the high-angle range, and more

307 especially for the 008:007 intensity ratio, even if the Debye-Waller factor of H_2O molecules is

308 maximized (B_{wat} = 10-11 Å^2).[44] In this case, the water content and the Δd parameter are

309 increased from 6.6 to 6.8 H_2O per $O_{20}(OH)_4$ and from 1.20 to 1.32 Å, respectively, as

310 compared to the 2WS configuration with B_{wat} = 2 Å^2 (Table 2). A 008:007 intensity ratio

311 consistent with that observed experimentally can be obtained by considering the 2WG

312 configuration for interlayer H_2O molecules. In this case, broad Gaussian distributions were

313 assumed (FWHM = 1.7 Å), and both the water content and the Δd parameter were increased

314 as compared to alternative interlayer configurations (Table 2). This 2WG configuration also

315 allows fitting better the profile of the 005 reflection, but that of the 003 one is slightly altered

316 as a result of a low-angle tail broadening (Figure 1e).

317 The combination of two structures, a main periodic one with only 2W layers and a

318 second one containing the three layer types (Table 1), accounts for the hydration

319 heterogeneity of sample Ca-SWy-2 at 40% RH, and leads to the coexistence of 2W, 1W, and

320 0W layers (95%, 4%, and 1%, respectively).[20] The 2WS configuration allows describing most

321 features of the experimental XRD patterns (R_p = 1.31% and R_{wp} = 8.13% − Figure 3a).

322 However, the 008 reflection is significantly more intense than the 007 one. By increasing the

323 Debye-Waller B_{wat} factor from 2 to 11 Å^2, the 008:007 intensity ratio appears closer to the

324 experimental one although the two estimates of the fit quality are not affected (Figure 3b).

325 This ratio is best reproduced by assuming a 2WG distribution with a FWHM of 1.4 Å (Figure

326 3c) although R_p and R_{wp} parameters are almost unaffected. As compared to the 2WS mode,

327 the total amount of H_2O molecules in such 2WG configuration is considerably increased from

328 6.2 (assuming a B_{wat} factor of 2 Å^2) to 7.8 per $O_{20}(OH)_4$ (Table 2).

329 *Sr-saturated montmorillonite.* At both 60 and 80% RH, the hydration heterogeneity of

330 sample Sr-SWy-1 is minimum as it contains an overwhelming proportion of 2W layers (95,

331 and 96%, respectively − Table 1).[18] As for the Ca-saturated samples, the 2WS configuration

332 for H_2O molecules leads to a satisfactory fit to the experimental XRD patterns, especially for

333 00ℓ reflections with ℓ<6, and for the 008 reflection (Figures 4a, 5a). However, significant

334 discrepancies between experimental and calculated patterns are visible for the 002 reflection

335 and the 008:007 intensity ratio. These discrepancies are significantly reduced by increasing

336 the Debye-Waller factor of H_2O molecules from 2 to 11 Å^2, but they do not vanish completely

337 (Figures 4b, 5b). The optimum fit to the experimental XRD patterns was again obtained

338 assuming a 2WG distribution of interlayer H_2O molecules with a large FWHM value (1.2, and

339 1.5 Å for Sr-SWy-1 samples recorded at 60 and 80% RH, respectively − Table 2; Figures 4c,

340 5c). For the two samples, both Rp and Rwp are lower for the 2WG configuration of interlayer

341 H_2O molecules than for the 2WS ones.

342 *Na-saturated montmorillonite*. At 80% RH, the Na-SWy-2 sample exhibits a high

343 proportion (92%) of 2W layers whereas minor amounts of 1W and 0W layers (5%, and 3%,

344 respectively) account for the hydration heterogeneity (Table 1). As for the previous sample,

345 the 2WS configuration of H_2O molecules leads to a satisfactory agreement between

346 experimental and calculated data, especially for 00ℓ reflections with ℓ<6, and for the 008

347 reflection (Figure 6a). However, by using a Debye-Waller factor of 2 $Å^2$ the intensity

348 calculated for the 006 and 007 reflections are too low as compared to the experimental one.

349 Increasing the B_{wat} factor up to 11 $Å^2$ significantly reduces these discrepancies although the

350 008:007 intensity ratio remains imperfectly reproduced (Figure 6b). The optimum fit to the

351 experimental data for this sample was again obtained assuming a 2WG distribution of H_2O

352 molecules (Figure 6c – R_{wp} = 5.33%, R_p = 2.59%). The Δd and FWHM parameters of this

353 2WG distribution are 1.50 Å and 1.4 Å, respectively (Table 2). A similar fit to the

354 experimental data (Figure 6d – R_{wp} = 5.34%, R_p = 2.57%) was obtained assuming the

355 distribution of interlayer species shown on Figure 7, while all other parameters were kept

356 constant (Table 1). This distribution was derived from the MC simulations performed using

357 the NVT ensemble. MC calculated distributions exhibit a single peak for the oxygen atoms,

358 and two for the hydrogen atoms, between the interlayer mid-plane and the surface of the 2:1

359 layer, and are characteristic of the presence of a single plane of H_2O molecules on either side

360 of the cation plane which is located in the center of the interlayer. The distance between the

361 maximum of the oxygen distribution and the maximum of the hydrogen distribution closer to

362 the 2:1 layer is ~1.0 Å which is the length of the O-H bond in the water molecule. This

363 indicates a preferential orientation of the H_2O molecules in the interlayer, with one of the O-H

364 bonds almost perpendicular to the surface of the 2:1 layer. Similar configurations of H_2O

365 molecules in the interlayer of octahedrally-substituted smectites have been previously

366 reported from IR spectroscopy results,[45] and from microscopic simulations.[24] As for all other

367 samples, the amount of interlayer H_2O molecules has to be increased, together with the Δd

368 parameter, as the positional distribution of these species increases (Table 2).

369   *Na-saturated synthetic saponites*. At 90% RH, the hydration heterogeneity of both

370   synthetic saponites is minimum as they exhibit an overwhelming proportion of 2W layers (94,

371   and 97% for Na-Sap$_{0.8}$ and Na-Sap$_{1.4}$ samples, respectively – Table 1). As compared to the

372   natural ones, these two synthetic samples present larger CSDS along the c* axis, as evidenced

373   by the sharpening of the 00ℓ reflections (Table 1 – Figures 8, 9). Layer thickness of 2W layers

374   decreases from 15.4 Å to 15.0 Å as the layer charge increases from 0.8 to 1.4 per $O_{20}(OH)_4$

375   (samples Na-Sap$_{0.8}$ and Na-Sap$_{1.4}$, respectively – Table 1). For both samples, the 2WS

376   configuration of H_2O molecules with $B_{wat} = 2$ Å^2 allows fitting satisfactorily 00ℓ reflections

377   with $\ell<6$ (Figures 8a, 9a). Increasing the Debye-Waller factor up to 11 Å^2 leads to a perfect fit

378   to the experimental data for the high-charge sample (Na-Sap$_{1.4}$ – Figure 9b),whereas

379   significant discrepancies are still observed between experimental and calculated patterns for

380   the low-charge sample (Na-Sap$_{0.8}$ - Figure 8b). For this latter sample, the optimum fit to the

381   experimental data was again obtained assuming a 2WG distribution of H_2O molecules in the

382   smectite interlayer with Δd and FWHM parameters (1.39 Å and 1.4 Å, respectively) similar to

383   those obtained for natural samples (Figure 8c – Table 2). For the Na-Sap$_{1.4}$ sample, a fit

384   similar to the one obtained with a 2WS distribution of H_2O molecules and a high B_{wat} factor

385   was obtained assuming a 2WG distribution of H_2O molecules (Figures 9b, 9c). However, the

386   FWHM parameter of this distribution is significantly lower (0.8 Å) than those typically

387   obtained for natural samples (1.2-1.7 Å – Table 2).

388

389   **Discussion**

390

391   **Shortcomings of the usual description of H$_2$O molecule positional disorder in 2W**

392   **smectite interlayers.** By accounting for smectite hydration heterogeneity, it is possible to

393   model experimental XRD patterns thus gaining additional insights into the structure of

394   smectite interlayers. It should be noted first that the initial assumption of identical properties

395   for all layers exhibiting the same hydration state and present in the different MLSs was

396   verified for all samples, thus validating the proposed description of smectite hydration

397   heterogeneity. In addition, the configuration of H_2O molecules within 2W smectite layers

398   commonly used for XRD pattern simulations can be discarded as it systematically leads to

399   major discrepancies between experimental and calculated profiles (Figure 10).[18-20]

400   Specifically, the use of this usual configuration systematically leads to poor fits to the

401   experimental XRD patterns for low-angle high-intensity reflections such as 003, 004, and 005

402   reflections (Figure 10). By contrast, the distribution of H_2O molecules within a single plane

403   on either side of the mid-plane interlayer (2WS configuration) allows both fitting the profiles

404   and reproducing the relative intensities of the 00ℓ reflections with $\ell<6$ (Figures 1c, 3a, 4a, 5a,

405   6a, 8a, 9a).[18] When assuming a Debye-Waller B_{wat} factor of 2 Å^2, this model leads to

406   significant discrepancies for high-order 00ℓ reflections, which are partly resolved by

407   increasing the positional disorder of H_2O molecules ($B_{wat} = 11$ Å^2 – Figures 1d, 3b, 4b, 5b,

408   6b, 8b, 9b). However, except for sample Na-Sap$_{1.4}$, such an increased B_{wat} factor does not

409   allow fitting satisfactorily the high-order 00ℓ reflections, which would require unrealistically

410   high B_{wat} factor values. In addition, the contrasting B_{wat} factors adjusted for the two synthetic

411   saponite samples recorded under similar RH conditions plead for a different origin to the

412   actual positional disorder of H_2O molecules in smectite interlayers.

413   **Distribution of H_2O molecules according to a double Gaussian function.** The 2WG

414   model can be considered as an improved version of the 2WS model in which the actual

415   positional disorder of H_2O molecules is better accounted for (Figures 1e, 3c, 4c, 5c, 6c, 8c,

416   9c). In the 2WG model the interlayer cation is considered to lie in a fixed position located in

417   the interlayer mid-plane and to have a Debye-Waller factor of 2 Å^2. This hypothesis does not

418   imply that the interlayer cations are not distributed as H_2O molecules are, but it was assumed

419   as a first approximation that thermal motion would be sufficient to account for their positional

420   disorder In addition, the sensitivity to the positional disorder of these cations is much reduced

421   as compared to H_2O molecules as the former species accounts for a minor part of the overall

422   electronic density in smectite interlayers. For example, at 80% RH Ca^{2+} cations account for

423   only 6% of the interlayer electrons (Table 3).

424   When comparing the electronic density due to interlayer H_2O molecules deduced from

425   MC calculations with that obtained from XRD profile fitting (Figure 11a), it is possible to

426   note that the overall profiles are globally alike in spite of significant differences. In particular

427   the two planes of H_2O molecules on either side of the interlayer mid-plane are much narrower

428   in the MC calculations (FWHM ~ 0.7 Å as compared to ~1.4 Å for XRD profile fitting) which

429   indicate also a significantly higher electron density in the interlayer mid-plane. The narrower

430   distribution obtained from the MC simulation can be due in part to the fixed interlayer

431   displacement between adjacent layers considered for the calculations although the influence

432   of interlayer shift and/or layer rotation on the distribution of interlayer species derived from

433   MC simulations is expected to be limited. The simple (simplistic ?) Gaussian functions used

434   to model the distribution of H_2O molecules are both shifted toward the interlayer mid-plane

435   (by about 0.2 Å) and broadened as compared to MC calculations. Both the broadening and the

436   shift of the Gaussian distributions are likely related to the specific profile of the MC

437   distribution, and more especially to the high electron density in the interlayer mid-plane

438   (Figure 7). However, the XRD profiles calculated assuming the two models are almost

439   identical (Figures 6c, 6d), pleading for a limited sensitivity of calculated XRD patterns to

440   these two parameters if the actual distribution profile is unknown.

441   *Validity of the 2WG configuration model.* Similar XRD patterns may be calculated

442   with 2WG and 2WS models by increasing the B_{wat} factor in the latter model (Figures 8c, 8d,

443   and 9b, 9c). Because of the demonstrated sensitivity of calculated XRD patterns to the

444   distribution of H₂O molecules, this similarity can only result from similar contributions of

445   H₂O molecules to the structure factor in both models. Factors affecting the structure factor

446   include the scattering power, the position and the amount of considered species. If the origin

447   of the layer unit is set in the center of the layer octahedron, the contribution of H₂O molecules

448   to the structure factor of 00ℓ reflections for a periodic 2W smectite (2WS model) can be

449   expressed as:

$$F_{H_2O}(00\ell) = 2n_{H_2O}\, f_B\left(\frac{\sin\theta}{\lambda}\right)_{00\ell} \cos(2\pi\ell Z) \tag{1}$$

451   where $f_B\left(\dfrac{\sin\theta}{\lambda}\right)_{00\ell}$ is the scattering power of H₂O molecules taking into account

452   their thermal motion (B$_{wat}$), n_{H_2O} is the amount of H₂O molecules at $Z = \dfrac{1}{2} - \dfrac{\Delta d}{h}$, h being

453   the layer thickness. Δd is the distance between the interlayer mid-plane and the positions of

454   the H₂O molecules along the c* axis. With increasing values of ℓ, the contribution of H₂O

455   molecules decreases together with $f_B(00\ell)$ as a result of the thermal motion of H₂O

456   molecules.

457   For the 2WG model, the contribution of interlayer H₂O molecules to the structure

458   factor of 00ℓ reflections for a periodic 2W smectite can be expressed as:

$$F_{H_2O}(00\ell) = 4 f\left(\frac{\sin\theta}{\lambda}\right)_{00\ell} \cos\left(2\pi\ell\left(\frac{1}{2} - \frac{\Delta d}{h}\right)\right) \sum_m n_m \cos\left(2\pi\ell m\frac{\Delta z}{h}\right) \tag{2}$$

460   where $f\left(\dfrac{\sin\theta}{\lambda}\right)_{00\ell}$ is the scattering power of H₂O molecules (B$_{wat}$ = 0), and Δd is the

461   distance along the c* axis between the interlayer mid-plane and the position of the maximum

462   density of the Gaussian distribution. n_m is the amount of H₂O molecules at a given distance

463   (mΔz, m being integer) from the maximum density of the Gaussian distribution. The sum

464   $\sum_m n_m$ equals the total number of interlayer H₂O molecules. For a given ℓ value, the

465 positional distribution of H_2O molecules disturbs their coherent scattering and thus decreases

466 their absolute contribution to the structure factor. The decrease becomes more important as

467 the ℓ indice increases. To quantify this decrease, Equation (2) can be expressed as:

468
$$F_{H_2O}(00\ell) = 2n_{H_2O}^{eff} f\left(\frac{\sin\theta}{\lambda}\right)_{00\ell} \cos\left(2\pi\ell\left(\frac{1}{2} - \frac{\Delta d}{h}\right)\right)\sum_m n_m \cos\left(2\pi\ell m\frac{\Delta Z}{h}\right) \qquad (3)$$

469 where $n_{H_2O}^{eff} = 2\sum_m n_m \cos\left(2\pi\ell m\frac{\Delta Z}{h}\right)$ is the effective amount of interlayer H_2O

470 molecules contributing to the structure factor. Equations (1) and (3) look similar but in the

471 sum determining the $n_{H_2O}^{eff}$ value, the cosine term is lower than 1, and $n_{H_2O}^{eff}$ is thus lower

472 than the total number of H_2O molecules. In addition, the $n_{H_2O}^{eff}$ value decreases with

473 increasing ℓ indices.

474   Thus both 2WS and 2WG models are essentially different although in both cases the

475 contribution of interlayer H_2O molecules to the structure factor is strongly decreasing with

476 increasing ℓ indices. In the first case, the thermal motion of these interlayer species is entirely

477 responsible for the decrease whereas in the latter model the decrease is related to the

478 decreasing effective number of H_2O molecules contributing to coherent diffraction effects.

479 Note that both models may produce similar diffraction effects if appropriate values are used

480 for the parameters describing the positional disorder of interlayer molecules. However,

481 unrealistically large values were obtained for the B_{wat} parameter when fitting Na-Sap$_{0.8}$

482 ($B_{wat} = 30$ Å^2) as compared to Na-Sap$_{1.4}$ ($B_{wat} = 11$ Å^2) although both XRD patterns were

483 recorded under similar experimental conditions, and the 2WG configuration of H_2O

484 molecules appears as more realistic than the 2WS one. Additional support for the 2WG model

485 arises from the close match between the number of interlayer H_2O molecules determined

486 using the 2WG model and that measured independently from water vapor isotherms.

487   *Water content in smectite interlayer*. For a given sample, the total amount of interlayer

488   H_2O molecules can be approximated by weighing the water content hypothesized for each

489   layer type by the relative abundance of this layer type and compared to that obtained from

490   water vapor adsorption-desorption isotherm experiments (Table 3).[18] The water content

491   determined by Ferrage et al. from XRD profile modeling assuming a 2WS model for the

492   distribution of interlayer H_2O molecules was reasonably consistent with that obtained from

493   water vapor adsorption-desorption isotherm experiments.[14,16,18] However, the 2WG

494   configuration provides the best agreement with the water contents determined experimentally

495   from water vapor adsorption-desorption isotherm experiments, the XRD values lying most

496   often between the values obtained on either branches of the isotherm (Tables 2, 3).

497   *FWHM of H_2O molecule Gaussian distribution.* When using the 2WG model to

498   describe the distribution of H_2O molecules in 2W layers, the FWHM parameter represents the

499   positional disorder of the species, which is characterized by the B_{wat} factor in usual models.

500   One may note that the diffraction effects resulting from the two configurations are similar and

501   lead to a significant decrease of the coherent scattering of H_2O molecules with increasing

502   diffraction angle (see above). However, the B_{wat} factor should be about constant for a given

503   species whereas the FWHM parameter can be structurally interpreted. For example, when

504   increasing the RH, the FWHM of the Gaussian distribution systematically increases for Ca-

505   and Sr-saturated montmorillonites (Table 2 – Figures 11b, 11c) most likely to accommodate

506   the steady addition of H_2O molecules weakly bound to the interlayer cation. On the contrary,

507   with increasing layer charge, Na-saturated saponite samples hold more H_2O molecules for a

508   given RH value in a narrower distribution (Figure 11d – Table 2). A possible origin for such

509   narrowing of H_2O molecule distributions is the increased polarization of these interlayer

510   species resulting from a stronger undersaturation of surface oxygen atoms.

511   *Relative positions of interlayer cations and H2O molecules.* The distance (Δd) between

512   the interlayer cations, which are located in the interlayer mid-plane, and the maximum density

513   of the interlayer H_2O molecule distribution function was also varied from one model to the

514   other, the maximum Δd values being obtained with the 2WG configuration of H_2O molecules

515   (Table 2). The Δd values reported in the present study represent only indicative values that

516   could be used for XRD profile modeling but a more complete study should be carried out to

517   determine the key factors that influence this parameter.

518   **Consistency with reported interlayer structures of expandable 2:1 phyllosilicates.**

519   *Comparison with the present data.* Among expandable 2:1 phyllosilicates, vermiculite

520   and smectite are differentiated from their contrasting layer charge, vermiculite exhibiting a

521   higher layer charge (1.2-1.8 per $O_{20}(OH)_4$) than smectite (0.4-1.2 per $O_{20}(OH)_4$).[46] This

522   difference is usually revealed by the contrasting swelling behavior of the two minerals after

523   magnesium saturation and glycerol solvation, vermiculite and smectite exhibiting basal

524   spacings of ~14 Å and ~18 Å, respectively, after such treatment.[1,47,48] However, distinct

525   hydration behavior has not been reported for these two mineral species, and the predominance

526   of bi-hydrated layers has been documented for the two species as a function of relative

527   humidity. As a consequence, these two expandable 2:1 phyllosilicates will be considered

528   together in the following.

529   For modeling XRD results of clay minerals containing 2W layers, the interlayer water

530   configuration usually assumed for bi-hydrated smectite is that used for the calculations

531   showed on Figures 1a and 10 and already described (Type I – Figure 12).[1] This model does

532   not allow the description of experimental XRD patterns (Figure 10) and may be rejected.

533   Most of the three-dimensional structural determinations of 2W interlayer

534   configuration were actually performed on vermiculite as this mineral frequently exhibits

535   ordered stacking sequences and because its higher content of interlayer cations allows for a

536　more accurate refinement of cation positions as compared to smectite. In addition vermiculite,

537　as illite, presents an ordered distribution of interlayer cations which eases the structural

538　characterization of the interlayer configuration as compared to smectite.[49] The structural

539　studies devoted to the configuration of interlayer species have led to different structure

540　models that will be described below.

541　　In bi-hydrated Mg-vermiculite, Mg^{2+} cations are located in the mid-plane of the

542　interlayer with one sheet of H_2O molecules on each side of this plane (Type II - Figure

543　12).[5,50,51,52,53] According to this model, Mg is octahedrally coordinated by six H_2O molecules

544　whereas additional H_2O molecules, which are weakly bound to the cation, are located on the

545　same plane as the six cation-bound H_2O molecules.[54-57] A Type II configuration of H_2O

546　molecules was also proposed for Na-saturated vermiculite,[58,59] and for Na-, Ca- and Li-rich

547　altered phlogopites.[60]

548　　A second configuration of interlayer species has been proposed for Ca-saturated

549　vermiculites (Type III – Figure 12).[58,61,62] In this model, two distinct coordinations are

550　reported for Ca^{2+} cations, two out of three Ca^{2+} cations being octahedrally coordinated as in

551　type II configuration, whereas remaining Ca^{2+} cations exhibit a cubic coordination. This dual

552　coordination induces the presence of two discrete planes of H_2O molecules (planes 2 and 3 –

553　Figure 12) in addition to that observed in the type II configuration, which holds most H_2O

554　molecules (plane 1 – Figure 12). The increased heterogeneity of H_2O configuration in Ca-,

555　Sr-, and Ba-saturated samples as compared to Mg-saturated ones was confirmed both from

556　diffraction and IR results.[56,57] A Type III configuration of H_2O molecules was also proposed

557　for Na-saturated vermiculite.[58] Figure 13 compares the 2WG configuration of interlayer H_2O

558　molecules determined for Ca-SWy-2 (40% RH) in the present study with that reported in the

559　literature for Ca-saturated vermiculite.[58,61] After normalization of the three distributions to the

560　denser plane of H_2O molecules, the three planes of H_2O molecules appear closely related to

561 the 2WG configuration proposed in the present study to describe the positional distribution of

562 interlayer species.

563   To compare the Δd values obtained in the present study with those reported in the

564 literature (1.14-1.45 Å – Table 4), these values can be normalized to the thickness of the

565 interlayer space to account better for the balance of the interactions with the interlayer cation

566 on the one hand and the 2:1 layer on the other hand (Table 5). Following such a normalization

567 procedure, the Δd values determined for the 2WG configuration of H_2O molecules are

568 consistent with those reported in the literature whereas lower values are obtained when

569 assuming a 2WS configuration.

570   In addition, z-coordinates along c* axis were recalculated together with typical

571 distances between the 2:1 layer and the planes of H_2O molecules, and between H_2O molecules

572 and interlayer cations (Table 4). For type II and III configurations the distance between the

573 2:1 layer and the densest plane of H_2O molecules scatters between 2.36 Å and 2.82 Å and is

574 consistent with the formation of H-bonds between interlayer H_2O molecules and the clay

575 framework. The distance between the densest plane of H_2O molecules and the interlayer

576 cation ranges from 1.14-1.45 Å.

577   *Specific interlayer structure resulting from the presence of tetrahedral substitutions.* A

578 third configuration of water in 2W smectite has been envisaged for Na-beidellite samples,

579 with Na^+ cations being partly engaged in the ditrigonal cavities of the 2:1 layers and the

580 coordinated H_2O molecules distributed on either side of the interlayer mid-plane which is

581 devoid of atoms (Type IV – Figure 12).[12,13,63] Such a migration of the interlayer cation from

582 the interlayer mid-plane toward the 2:1 clay framework is consistent with MC simulations and

583 IR spectroscopy results which both support the formation of inner-sphere complexes for

584 monovalent cations in tetrahedrally substituted 2:1 phyllosilicates.[21,24,26,31] In the present

585 study, similar distributions of interlayer species have been determined whatever the location

24

586 of the layer charge deficit in agreement with previous reports of Type II and Type III

587 configurations of interlayer species in tetrahedrally substituted 2W vermiculites.[58-60] The

588 central location of Na^+ cations was found to be consistent with experimental XRD data even

589 when Na^+ cations account for a significant part of the interlayer electronic density (13% of the

590 interlayer electrons for sample Na-Sap$_{1.4}$). Furthermore, if a Type IV configuration is assumed

591 for the distribution of interlayer species, significant discrepancies arise between experimental

592 and calculated patterns, especially for the 002 and 003 reflections which are extremely

593 sensitive to the presence of interlayer species at the interlayer mid-plane position (Figure 14).

594 In conclusion, the present data does not provide experimental evidence for the migration of

595 monovalent cations toward the surface of tetrahedrally substituted 2:1 layers.

596

606

607 **Literature cited**

608

609　　　　(1)　　　Moore, D. M.; Reynolds, R. C., Jr *X-ray Diffraction and the Identification and*

610　*Analysis of Clay Minerals*; Oxford University Press: Oxford and New York, 1997.

611　　　　(2)　　　Nagelschmidt, G. *Z. Kristallogr.* **1936**, *93*, 481-487.

612　　　　(3)　　　Bradley, W. F.; Grim, R. E.; Clark, G. F. *Z. Kristallogr.* **1937**, *97*, 260-270.

613　　　　(4)　　　Mooney, R. W.; Keenan, A. G.; Wood, L. A. *J. Am. Chem. Soc.* **1952**, *74*,

614　1371-1374.

615　　　　(5)　　　Walker, G. F. *Clays & Clay Miner.* **1956**, *4*, 101-115.

616　　　　(6)　　　Norrish, K. *Discuss. Faraday Soc.* **1954**, *18*, 120-133.

617　　　　(7)　　　Van Olphen, H. *J. Colloid Sci.* **1965**, *20*, 822-837.

618　　　　(8)　　　Kittrick, J. A. *Soil Sci. Soc. Am. J.* **1969a**, *33*, 217-222.

619　　　　(9)　　　Kittrick, J. A. *Soil Sci. Soc. Am. J.* **1969b**, *33*, 222-225.

620　　　　(10)　　Laird, D. A. *Clays & Clay Miner.* **1996**, *44*, 553-559.

621　　　　(11)　　Laird, D. A. *Clays & Clay Miner.* **1999**, *47*, 630-636.

622　　　　(12)　　Ben Brahim, J.; Besson, G.; Tchoubar, C. In *5th Meeting of the European Clay*

623　*Groups*: Prague, 1983, pp 65-75.

624　　　　(13)　　Ben Brahim, J.; Besson, G.; Tchoubar, C. *J. Appl. Cryst.* **1984**, *17*, 179-188.

625　　　　(14)　　Bérend, I.; Cases, J. M.; François, M.; Uriot, J. P.; Michot, L. J.; Masion, A.;

626　Thomas, F. *Clays & Clay Miner.* **1995**, *43*, 324-336.

627　　　　(15)　　Cases, J. M.; Bérend, I.; Besson, G.; François, M.; Uriot, J. P.; Thomas, F.;

628　Poirier, J. P. *Langmuir* **1992**, *8*, 2730-2739.

629　　　　(16)　　Cases, J. M.; Bérend, I.; François, M.; Uriot, J. P.; Michot, L. J.; Thomas, F.

630　*Clays & Clay Miner.* **1997**, *45*, 8-22.

631　　　　(17)　　Cuadros, J. *Amer. J. Sci.* **1997**, *297*, 829-841.

632　　　　(18)　　Ferrage, E.; Lanson, B.; Sakharov, B. A.; Drits, V. A. *Amer. Mineral.* **2005**, in

633　press Ms #1776R.

634   (19)   Ferrage, E.; Lanson, B.; Sakharov, B. A.; Geoffroy, N.; Drits, V. A. *Amer.*

635   *Mineral.* **2005**, in preparation.

636   (20)   Ferrage, E.; Tournassat, C.; Rinnert, E.; Lanson, B. *Geochim. Cosmochim.*

637   *Acta* **2005**, in press Ms #2963.

638   (21)   Skipper, N. T.; Chang, F. R. C.; Sposito, G. *Clays & Clay Miner.* **1995**, *43*,

639   285-293.

640   (22)   Chang, F. R. C.; Skipper, N. T.; Sposito, G. *Langmuir* **1998**, *14*, 1201-1207.

641   (23)   Boek, E. S.; Coveney, P. V.; Skipper, N. T. *J. Am. Chem. Soc.* **1995**, *117*,

642   12608-12617.

643   (24)   Chang, F. R. C.; Skipper, N. T.; Sposito, G. *Langmuir* **1995**, *11*, 2734-2741.

644   (25)   Chang, F. R. C.; Skipper, N. T.; Sposito, G. *Langmuir* **1997**, *13*, 2074-2082.

645   (26)   Skipper, N. T.; Sposito, G.; Chang, F. R. C. *Clays & Clay Miner.* **1995**, *43*,

646   294-303.

647   (27)   Skipper, N. T.; Refson, K.; McConnell, J. D. C. *J. Chem. Phys.* **1991**, *94*, 7434-

648   7445.

649   (28)   Greathouse, J.; Refson, K.; Sposito, G. *J. Am. Chem. Soc.* **2000**, *122*, 11459-

650   11464.

651   (29)   Sposito, G.; Skipper, N. T.; Sutton, R.; Park, S. H.; Soper, A. K.; Greathouse,

652   J. A. *Proc. Nat. Acad. Sci. USA* **1999**, *96*, 3358-3364.

653   (30)   Michot, L. J.; Villiéras, F. *Clay Miner.* **2002**, *37*, 39-57.

654   (31)   Pelletier, M.; Michot, L. J.; Humbert, B.; Barres, O.; D'espinose de la Callerie,

655   J. B.; Robert, J. L. *Amer. Mineral.* **2003**, *88*, 1801-1808.

656   (32)   Drits, V. A.; Sakharov, B. A. *X-Ray structure analysis of mixed-layer minerals*;

657   Dokl. Akad. Nauk SSSR: Moscow, 1976.

658   (33)   Drits, V. A.; Lindgreen, H.; Sakharov, B. A.; Salyn, A. S. *Clay Miner.* **1997**,

659   *33*, 351-371.

660   (34)   Sakharov, B. A.; Lindgreen, H.; Salyn, A.; Drits, V. A. *Clays & Clay Miner.*

661   **1999**, *47*, 555-566.

662   (35)   Drits, V. A.; Srodon, J.; Eberl, D. D. *Clays & Clay Miner.* **1997**, *45*, 461-475.

663   (36)   Guinier, A. *Théorie et technique de la radiocristallographie*; Dunod: Paris,

664   1964.

665   (37)   Drits, V. A.; Tchoubar, C. *X-ray diffraction by disordered lamellar structures:*

666   *Theory and applications to microdivided silicates and carbons*; Springer-Verlag: Berlin,

667   1990.

668   (38)   Howard, S. A.; Preston, K. D. In *Modern Powder Diffraction*; Bish, D. L.,

669   Post, J. E., Eds.; Mineralogical Society of America: Wahington D.C., 1989; Reviews in

670   Mineralogy Vol. 20, pp 217-275.

671   (39)   Plançon, A. *Amer. Mineral.* **2002**, *87*, 1672-1677.

672   (40)   Marry, V., *Ph.D. dissertation*, Pierre et Marie Curie University - Paris, 2002.

673   (41)   Marry, V.; Turq, P.; Cartailler, T.; Levesque, D. *J. Chem. Phys.* **2002**, *117*,

674   3454-3463.

675   (42)   Delville, A. *Langmuir* **1992**, *8*, 1796-1805.

676   (43)   Boek, E. S.; Coveney, P. V. ; Skipper, N. T. *Langmuir* **1995**, *11*, 4629-4631.

677   (44)   Lipson, H. In *International tables for X-ray crystallography*;; Casper, J. S.,

678   Lonsdale, K., Eds., 1967; International Union of Crystallography; Mathematical tables Vol. 2

679   - Mathematical tables, pp 235-315.

680   (45)   Sposito, G.; Prost, R. *Chem. Rev.* **1982**, *82*, 553-573.

681   (46)   Bailey, S. W. *Clay Miner.* **1980**, *15*, 85-93.

682   (47)   Calle, C. de la; Suquet, H. In *Hydrous Phyllosilicates (exclusive of micas)*;

683   Bailey, S. W., Ed.; Mineralogical Society of America: Washington, D.C., 1988; Reviews in

684   Mineralogy Vol. 19, pp 455-496.

685   (48)   Walker, G. F. *Clay Miner. Bull.* **1958**, *3*, 302-313.

686   (49)   Besson, G.; Misfud, A.; Tchoubar, C.; Méring, J. *Clays & Clay Miner.* **1974**,

687   *22*, 379-384.

688   (50)   Mathieson, A. M.; Walker, G. F. *Amer. Mineral.* **1954**, *39*, 231-255.

689   (51)   Mathieson, A. M. *Amer. Mineral.* **1958**, *43*, 216-227.

690   (52)   Bradley, W. F.; Serratosa, J. M. In *Clays & Clay Minerals, Proceeding of the*

691   *7th Clay Conference*; Pergamon Press, 1960, pp 260-270.

692   (53)   Shirozu, H.; Bailey, S. W. *Amer. Mineral.* **1966**, *51*, 1124-1143.

693   (54)   Alcover, J. F.; Gatineau, L.; Méring, J. *Clays & Clay Miner.* **1973**, *21*, 131-

694   136.

695   (55)   Alcover, J. F.; Gatineau, L. *Clay Miner.* **1980**, *15*, 25-35.

696   (56)   Alcover, J. F.; Gatineau, L. *Clay Miner.* **1980**, *15*, 239-248.

697   (57)   Fornés, V.; Calle, C. de la; Suquet, H.; Pezerat, H. *Clay Miner.* **1980**, *15*, 399-

698   411.

699   (58)   Slade, P. G.; Stone, P. A.; Radoslovitch, E. W. *Clays & Clay Miner.* **1985**, *33*,

700   51-61.

701   (59)   Beyer, J.; Graf von Reichenbach, H. *Clay Miner.* **2002**, *37*, 157-168.

702   (60)   Le Renard, J.; Mamy, J. *Bull. Groupe Franç. Argiles* **1971**, *23*, 119-127.

703   (61)   Calle, C. de la; Pezerat, H.; Gasperin, M. *J. Phys.* **1977**, *C7*, 128-133.

704   (62)   Calle, C. de la; Suquet, H.; Dubernat, J.; Pezerat, H. *Clay Miner.* **1978**, *13*,

705   275-197.

706   (63)   Ben Brahim, J.; Armagan, N.; Besson, G.; Tchoubar, C. *J. Appl. Cryst.* **1983**,

707   *16*, 264-269.

Figure captions

709

710 **Figure 1**. Comparison between experimental and calculated XRD patterns for the Ca-

711 saturated SWy-1 montmorillonite sample recorded at 80% RH. Structural parameters used for

712 the calculations are listed in Tables 1, 2, and 3. Experimental data are shown as crosses

713 whereas calculated profiles are shown as solid lines. Solid arrows indicate a significant misfit

714 between experimental and calculated patterns, whereas gray and open arrows indicate poor

715 and good fits, respectively. 00ℓ reflections are indexed in parentheses. (a) Calculation for a

716 periodic bi-hydrated structure (layer thickness of 2W layers = 15.48 Å) assuming the usual

717 configuration of H_2O molecules.[1] (b) Calculation for a periodic bi-hydrated structure (layer

718 thickness of 2W layers: 15.48 Å) assuming a 2WS configuration (see text for details) with

719 $B_{wat} = 2$ Å^2 for H_2O molecules.[18] (c) Calculation performed accounting for hydration

720 heterogeneities and assuming a 2WS configuration with $B_{wat} = 2$ Å^2 for H_2O molecules.[18]

721 Hydration heterogeneity was described by assuming the coexistence of a major MLS

722 containing 2W and 1W layers (95:5 ratio) and of a second structure containing the three layer

723 types (2W:1W:0W = 85:13:2) in a 61:39 ratio (Table 2). (d) Calculation performed

724 accounting for hydration heterogeneities and assuming a 2WS configuration with $B_{wat} = 11$ Å^2

725 for H_2O molecules. (e) Calculation performed accounting for hydration heterogeneities and

726 assuming a 2WG configuration (see text for details).

727 **Figure 2**. Relative intensities of 00ℓ reflections, after normalization to the 001 reflection, as a

728 function of structural parameters specific to the 2WG configuration (see text for details). The

729 total amount of H_2O molecules (nH_2O) is given per $O_{20}(OH)_4$, whereas the full width at half

730 maximum intensity (FWHM) of the distribution and the distance, in projection along the c*

731 axis, from its maximum to the interlayer mid-plane (Δd) are given in Å.

732   **Figure 3**. Comparison between experimental and calculated XRD patterns for the Ca-

733   saturated SWy-2 montmorillonite sample recorded at 40% RH. Structural parameters used for

734   the calculations are listed in Tables 1, 2, and 3. Patterns as for Figure 1. * indicates hk bands,

735   whereas vertical ticks denote the presence of accessory quartz reflections. (a) Calculation

736   performed assuming a 2WS configuration with $B_{wat} = 2$ Å^2 for H_2O molecules.[18] (b)

737   Calculation performed assuming a 2WS configuration with $B_{wat} = 11$ Å^2 for H_2O molecules.

738   (c) Calculation performed assuming a 2WG configuration.

739   **Figure 4**. Comparison between experimental and calculated XRD patterns for the Sr-saturated

740   SWy-1 montmorillonite sample recorded at 60% RH. Structural parameters used for the

741   calculations are listed in Tables 1, 2, and 3. Patterns as for Figure 1. (a) Calculation performed

742   assuming a 2WS configuration with $B_{wat} = 2$ Å^2 for H_2O molecules.[18] (b) Calculation

743   performed assuming a 2WS configuration with $B_{wat} = 11$ Å^2 for H_2O molecules. (c)

744   Calculation performed assuming a 2WG configuration.

745   **Figure 5**. Comparison between experimental and calculated XRD patterns for the Sr-saturated

746   SWy-1 montmorillonite sample recorded at 80% RH. Structural parameters used for the

747   calculations are listed in Tables 1, 2, and 3. Patterns as for Figure 1. (a) Calculation performed

748   assuming a 2WS configuration with $B_{wat} = 2$ Å^2 for H_2O molecules.[18] (b) Calculation

749   performed assuming a 2WS configuration with $B_{wat} = 11$ Å^2 for H_2O molecules. (c)

750   Calculation performed assuming a 2WG configuration.

751   **Figure 6**. Comparison between experimental and calculated XRD patterns for the Na-

752   saturated SWy-2 montmorillonite sample recorded at 80% RH. Structural parameters used for

753   the calculations are listed in Tables 1, 2, and 3. Patterns as for Figures 1 and 3. (a) Calculation

754   performed assuming a 2WS configuration with $B_{wat} = 2$ Å^2 for H_2O molecules.[18] (b)

755   Calculation performed assuming a 2WS configuration with $B_{wat} = 11$ Å^2 for H_2O molecules.

756   (c) Calculation performed assuming a 2WG configuration. (d) Calculation performed

757   assuming the distribution of interlayer species derived from MC simulations using the NVT

758   ensemble and shown in Figure 7.

759   **Figure 7**. Density profiles of interlayer species along the c* axis derived from MC

760   simulations performed using the NVT ensemble. z-coordinates are given in Å with the origin

761   located in the interlayer mid-plane. Solid, dashed and gray lines represent O, H, and Na^+

762   atoms, respectively.

763   **Figure 8**. Comparison between experimental and calculated XRD patterns for the Na-

764   saturated $Sap_{0.8}$ saponite sample recorded at 90% RH. Structural parameters used for the

765   calculations are listed in Tables 1, 2, and 3. Patterns as for Figure 1. (a) Calculation performed

766   assuming a 2WS configuration with $B_{wat} = 2$ $Å^2$ for H_2O molecules.[18] (b) Calculation

767   performed assuming a 2WS configuration with $B_{wat} = 11$ $Å^2$ for H_2O molecules. (c)

768   Calculation performed assuming a 2WG configuration. (d) Calculation performed assuming a

769   2WS configuration with $B_{wat} = 30$ $Å^2$ for H_2O molecules, 10.5 nH_2O molecules per $O_{20}(OH)_2$)

770   in 2W layers, and $\Delta d = 1.38$ Å.

771   **Figure 9**. Comparison between experimental and calculated XRD patterns for the Na-

772   saturated $Sap_{1.4}$ saponite sample recorded at 90% RH. Structural parameters used for the

773   calculations are listed in Tables 1, 2, and 3. Patterns as for Figure 1. (a) Calculation performed

774   assuming a 2WS configuration with $B_{wat} = 2$ $Å^2$ for H_2O molecules.[18] (b) Calculation

775   performed assuming a 2WS configuration with $B_{wat} = 11$ $Å^2$ for H_2O molecules. (c)

776   Calculation performed and assuming a 2WG configuration.

777   **Figure 10**. Comparison between experimental XRD patterns and those calculated assuming

778   the usual configuration of H_2O molecules.[1] Hydration heterogeneity has been taken into

779   account for all calculations. Structural parameters used for the calculations are listed in Table

780   1. Patterns as for Figures 1 and 3. (a) Ca-saturated SWy-1 montmorillonite sample recorded at

781   80% RH. (b) Ca-saturated SWy-2 montmorillonite sample recorded at 40% RH. (c) Sr-

782   saturated SWy-1 montmorillonite sample recorded at 60% RH. (d) Sr-saturated SWy-1

783   montmorillonite sample recorded at 80% RH. (e) Na-saturated SWy-2 montmorillonite

784   sample recorded at 80% RH. (f) Na-saturated $Sap_{0.8}$ saponite sample recorded at 90% RH. (g)

785   Na-saturated $Sap_{1.4}$ saponite sample recorded at 90% RH.

786   **Figure 11**. Density profiles along the c* axis of the electron distribution in the interlayer of

787   bi-hydrated smectite layers. z-coordinates are given in Å with the origin located in the

788   interlayer mid-plane. (a) Comparison between the electron distribution derived from the

789   density profiles of interlayer species calculated using the NVT ensemble (Figure 7) and the

790   one determined from XRD profile modeling for the Na-SWy-2 montmorillonite sample (80%

791   RH). (b) Comparison between the electron distributions determined from XRD profile

792   modeling for the two Ca-saturated montmorillonite samples under different RH conditions.

793   (c) Comparison between the electron distributions determined from XRD profile modeling for

794   the two Sr-saturated SWy-1 montmorillonite samples under different RH conditions. (d)

795   Comparison between the electron distributions determined from XRD profile modeling for

796   the two Na-saturated synthetic saponite samples with different amounts of layer charge.

797   **Figure 12**. Schematic description of the different configurations proposed in the literature for

798   interlayer species in 2W smectite layers. O and T refer to the octahedral and tetrahedral sheets

799   of the 2:1 layer, respectively. Labels of the different sheets of H_2O molecules are detailed in

800   the text.

801   **Figure 13**. Comparison of the distributions of H_2O molecules reported for bi-hydrated

802   smectites. The distributions are normalized to the denser plane of H_2O molecules, and z-

803   coordinates are given in fraction of the interlayer with the origin located in the interlayer mid-

804   plane after normalization to the interlayer thickness. The distribution determined from XRD

805   profile modeling for the Ca-saturated SWy-2 montmorillonite sample (40% RH) is plotted as

806   a solid line, whereas data from De la Calle et al. and from Slade et al. are shown as dashed

807   and dotted-dashed lines, respectively.[58,61]

808   **Figure 14**. Comparison between experimental and calculated XRD patterns for the Na-

809   saturated $Sap_{1.4}$ saponite sample recorded at 90% RH. Structural parameters used for the

810   calculations are listed in Tables 1, 2, and 3. Patterns as for Figure 1. Calculation is performed

811   assuming a Type IV configuration of interlayer species with a shift of the interlayer cation

812   from the interlayer mid-plane toward the 2:1 clay framework.[13]

813

Table 1. Optimum structural parameters used for the simulation of experimental XRD profiles.

Sample	Rel. ab. (%)[a]	2W[b]	1W[b]	0W[b]	L. Tck. 2W[c]	L. Tck. 1W[c]	L. Tck. 0W[c]	nH_2O 1W[d]	N[e]	σ*[f]	$σ_z$[g]
Ca-SWy-2 (40%RH)[h]	87	100	0	0	15.18	12.60	10.00	3.2	8.7	6.5	0.35
	13	60	30	10							
Ca-SWy-1 (80%RH)[i]	61	95	5	0	15.51	12.85	10.00	3.3	6.0	6.5	0.27
	39	85	13	2							
Sr-SWy-1 (60%RH)[i]	82	100	0	0	15.53	12.58	10.00	3.5	7.5	5.5	0.35
	18	75	15	10							
Sr-SWy-1 (80%RH)[i]	84	100	0	0	15.73	12.70	10.00	5.5	7.5	5.5	0.35
	16	75	15	10							
Na-SWy-2 (80%RH)	90	96	2	2	15.52	12.55	9.60	3.2	8.2	11.0	0.25
	10	60	30	10							
Na-Sap$_{0.8}$ (90%RH)	44	100	0	0	15.40	13.20	9.80	5.7	13.0	2.0	0.19
	56	90	5	5							
Na-Sap$_{1.4}$ (90%RH)	91	100	0	0	15.00	12.90	9.80	5.0	12.0	11	0.12
	9	70	20	10							

[a] Relative proportion of the different contributions to the diffracted intensity. [b] Relative proportion of the different layer types in the different contributions to the diffracted intensity. 2W, 1W, and 0W stand for bi-hydrated, mono-hydrated and de-hydrated smectite layers, respectively. [c] Layer thickness (L. Tck.) of the different layer types. [d] Number of H_2O molecules in 1W layers (per $O_{20}(OH)_4$). [e] Mean thickness of the coherent scattering domain size along the c* axis (in layers). [f] Sigmastar parameter characterizing the sample orientation (in °).[1] [g] Standard deviation of the layer thickness parameter (in Å).[18] [h] Data from Ferrage et al.[20] [i] Data from Ferrage et al.[18]

Table 2. Structural parameters of the interlayer space determined from XRD profile modeling as a function of the assumed water configuration.

Sample	2WS, $B_{wat} = 2$ [a]		2WS, $B_{wat} = 11$ [a]		2WG [b]		
	nH_2O [c]	Δd [d]	nH_2O	Δd	nH_2O	Δd	FWHM [e]
Ca-SWy-2 (40%RH)	6.2	1.20	6.6	1.30	7.8	1.34	1.4
Ca-SWy-1 (80%RH)	6.6	1.20	6.8	1.32	10.0	1.37	1.7
Sr-SWy-1 (60%RH)	6.0	1.20	6.8	1.32	8.5	1.40	1.2
Sr-SWy-1 (80%RH)	6.0	1.20	7.0	1.41	9.5	1.52	1.5
Na-SWy-2 (80%RH)	7.4	1.20	8.2	1.41	9.5	1.50	1.4
Na-Sap$_{0.8}$ (90%RH)	8.5	1.20	9.3	1.33	10.5	1.39	1.4
Na-Sap$_{1.4}$ (90%RH)	8.4	1.20	9.0	1.33	9.4	1.35	0.8

[a] 2WS corresponds to an interlayer configuration of H_2O molecules distributed as one plane on either side of the interlayer mid-plane. The Debye-Waller temperature factor for water (B_{wat}) given in $Å^2$. [b] 2WG corresponds to an interlayer configuration of H_2O molecules distributed according to a Gaussian function on either side of the interlayer mid-plane. [c] The number of H_2O molecules is given per $O_{20}(OH)_4$. In this case, $B_{wat} = 0$ $Å^2$. [d] The distance, in projection along the c* axis, between the interlayer mid-plane and the maximum density of the distribution of H_2O molecules (Δd) is given in $Å$. [e] The width of the Gaussian distribution of interlayer H_2O molecules (FWHM) is given in $Å$.

Table 3. Optimum amounts of H_2O molecules determined from XRD profile modeling for the different configurations of interlayer species, and from water vapor adsorption/desorption isotherms.

Sample	Type I configuration[a]	2WS $B_{wat} = 2$[b]	2WS $B_{wat} = 11$[b]	2WG[c]	Ads./Des.[d]
Ca-SWy-2 (40%RH)	7.25[e]	8.32	8.58	10.11	8.62/10.17
Ca-SWy-1 (80%RH)	7.06	8.30	8.54	12.36	12.85/13.70
Sr-SWy-1 (60%RH)	7.06	7.60	8.85	10.72	7.87/9.29 (10.70/11.90)
Sr-SWy-1 (80%RH)	7.14	7.69	8.95	12.09	9.83/10.45 (12.80/13.70)
Na-SWy-2 (80%RH)	7.04	9.27	10.24	11.82	10.50/13.10
Na-Sap$_{0.8}$ (90%RH)	7.00	10.62	11.60	13.07	13.39/14.49[f]
Na-Sap$_{1.4}$ (90%RH)	6.96	10.45	11.19	11.62	14.23/17.18[f]

[a] Interlayer configuration of H_2O molecules commonly used for the calculation XRD profiles including 2W layers.[1] [b] 2WS corresponds to an interlayer configuration of H_2O molecules distributed as one plane on either side of the interlayer mid-plane. The Debye-Waller temperature factor for water (B_{wat}) given in $Å^2$. [c] 2WG corresponds to an interlayer configuration of H_2O molecules distributed according to a Gaussian function on either side of the interlayer mid-plane. In this case, $B_{wat} = 0$ $Å^2$. [d] Water amounts determined experimentally from water vapor adsorption/desorption isotherms. Data are taken from Cases et al.,[16] and from Bérend et al.[14] for divalent and monovalent cations, respectively. [e] The water contents are given in mmol of water per g of clay. [f] Personal communication from Laurent Michot (LEM, Nancy, France).

Table 4. Structural parameters of the different configurations reported in the literature for interlayer water in bi-hydrated smectite layers.
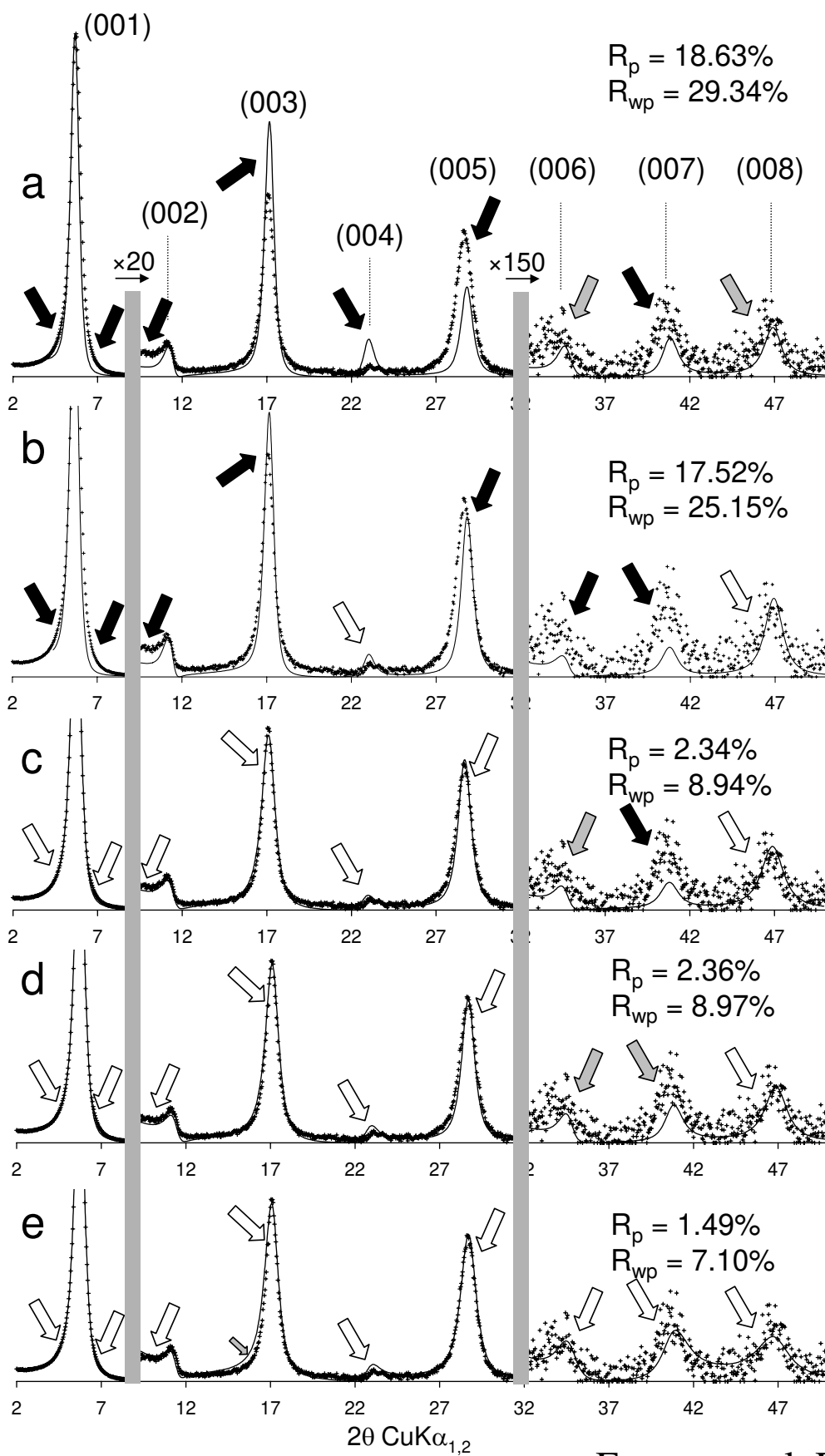
Type I configuration[a]					
Reference	Sample	Cation-$H_2O_{(iii)}$[b]	Cation-$H_2O_{(ii)}$[b]	Cation-$H_2O_{(i)}$[b]	B_{wat}[c,d]
Moore and Reynolds[1]	2W-Smectite	1.20	1.06	0.35	11/2§

Type II configuration					
Reference	sample	O_{layer}-H_2O[b]	Cation-H_2O[b]	d_{001}[e]	$nH_2O/nCat$[f]	B_{wat}[c]
Mathieson et al.[51]	Mg-Vermiculite	2.76	1.14	14.34	-	5.4
Shirozu et al.[53]	Mg-Vermiculite	2.67[g]	1.17[g]	14.33	7.44	6.1
Alcover et al.[55]	Mg-Vermiculite	2.69	1.19	14.36	-	-
Le Renard et al.[60]	Altered Ca-Phlogopite	2.77	1.41	14.96	8.60	-
	Altered Na-Phlogopite	2.71	1.43	14.87	10.70	-
	Altered Li-Phlogopite	2.71	1.30	14.62	8.79	-
Beyer et al.[59]	Na-Vermiculite	2.70[g]	1.44[g]	14.85	4.00	3.9

Type III configuration					
Reference	Sample	O_{layer}-H_2O[b,h]	Cation-H_2O[b,h]	d_{001}[e]	$nH_2O/nCat$[f]	B_{wat}[c]
De la Calle et al.[61]	Ca-Vermiculite	2.78	1.45[f]	14.92	7.34	5.5
Slade et al.[58]	Ca-Vermiculite	2.82	1.41[f]	14.89	8.02	2.5
	Na-Vermiculite	2.66	1.42	14.85	5.58	3.9

Type IV configuration						
Reference	Sample	O_{layer}-H_2O[b]	O_{layer}-Cation[b]	Cation-H_2O[b]	d_{001}[e]	$nH_2O/nCat$[f]	B_{wat}[c]
Ben Brahim et al.[13]	Na-Beidellite	3.00	1.00	2.00	15.25	11.87	5

[a] Configurations of interlayer water in bi-hydrated smectite layers are schematized on Figure 2. [b] Distances are measured in projection along the c* axis and given in Å. O_{layer}, H_2O, and cation stand for the outermost plane of oxygen from the 2:1 layer, the H_2O molecules and the interlayer cations, respectively. [c] B_{wat} is the Debye-Waller temperature factor reported for H_2O molecules (in Å^2). [d] Debye-Waller factor is 11 Å^2 for plane (iii) and 2 Å^2 for planes (i) and (ii), respectively. [e] Basal distance d_{001} along the c* axis is given in Å. [f] $nH_2O/nCat$ represents the ratio between the number of interlayer H_2O molecules and that of interlayer cations. [g] Average value for the different planes of H_2O molecules. [h] Distances are given for the denser plane of H_2O molecules.
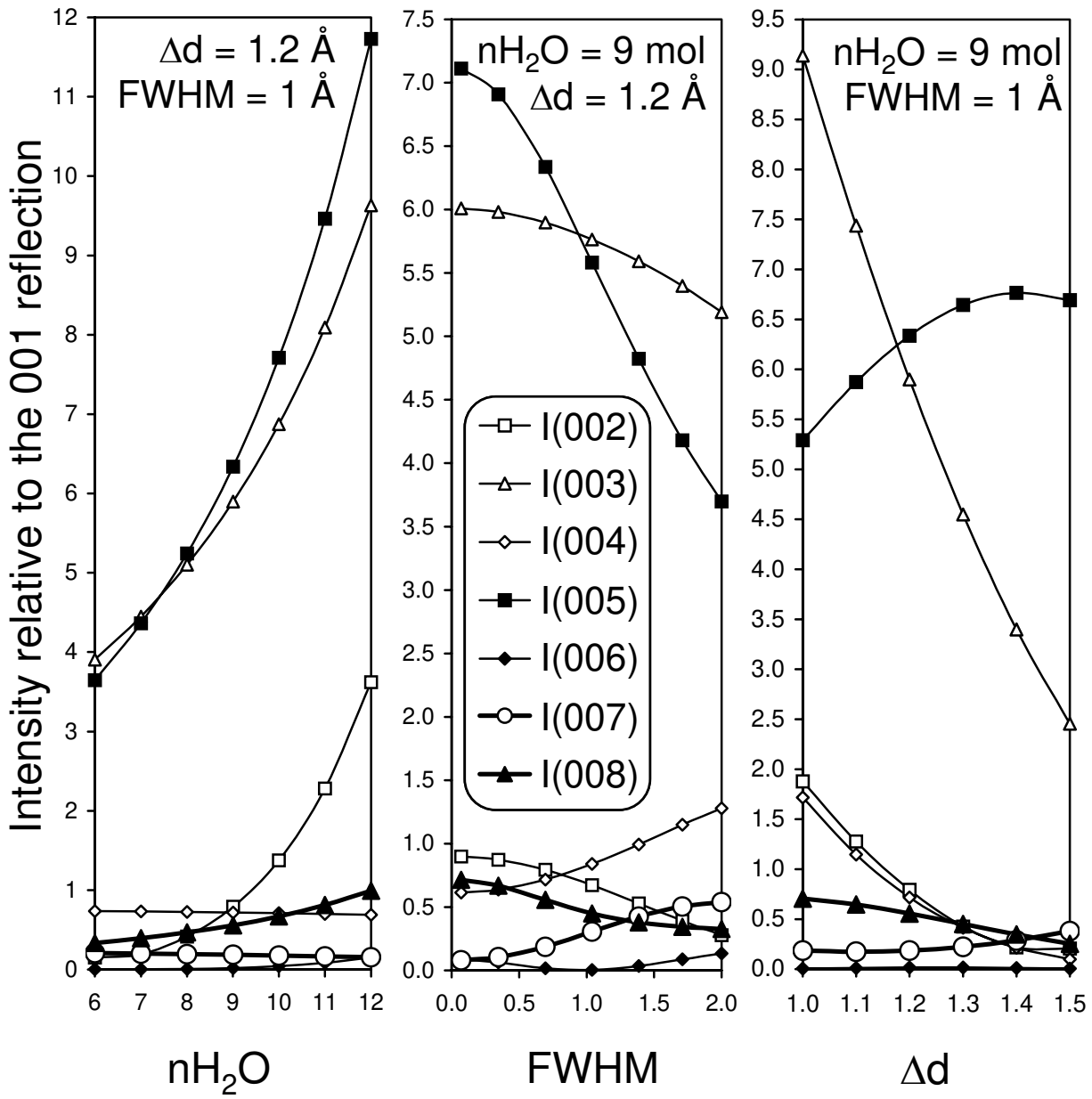
Table 5. Distances along the c* axis between the interlayer mid-plane and the maximum density of the H_2O molecule distribution normalized to the thickness of the interlayer space for the different configurations of interlayer species.

Sample	2WS, $B_{wat} = 2$[a]	2WS, $B_{wat} = 11$[a]	2WG[b]
Ca-SWy-2 (40%RH)	27.8%[c]	30.1%	31.0%
Ca-SWy-1 (80%RH)	26.8%	29.4%	30.5%
Sr-SWy-1 (60%RH)	26.7%	29.4%	31.1%
Sr-SWy-1 (80%RH)	26.1%	30.7%	33.1%
Na-SWy-2 (80%RH)	26.7%	31.4%	33.4%
Na-Sap$_{0.8}$ (90%RH)	27.1%	30.0%	31.4%
Na-Sap$_{1.4}$ (90%RH)	28.4%	31.4%	31.9%
Mean value	27.1% ± 0.7%	30.3% ± 0.8%	31.8% ± 1.0%
Literature mean value[d]		32.7% ± 2.1%	

[a] 2WS corresponds to an interlayer configuration of H_2O molecules distributed as one plane on either side of the interlayer mid-plane. The Debye-Waller temperature factor for water (B_{wat}) given in $Å^2$. [b] 2WG corresponds to an interlayer configuration of H_2O molecules distributed according to a Gaussian function on either side of the interlayer mid-plane. [c] The distance along the c* axis between the interlayer mid-plane and the maximum density of the H_2O molecule distribution (Δd) is normalized to the thickness of the interlayer (L. Tck. minus the thickness of the 2:1 layer – 6.54 Å). [d] Average value calculated from the data reported for Type II and Type III configurations of interlayer species.[51,53,55,58-61]
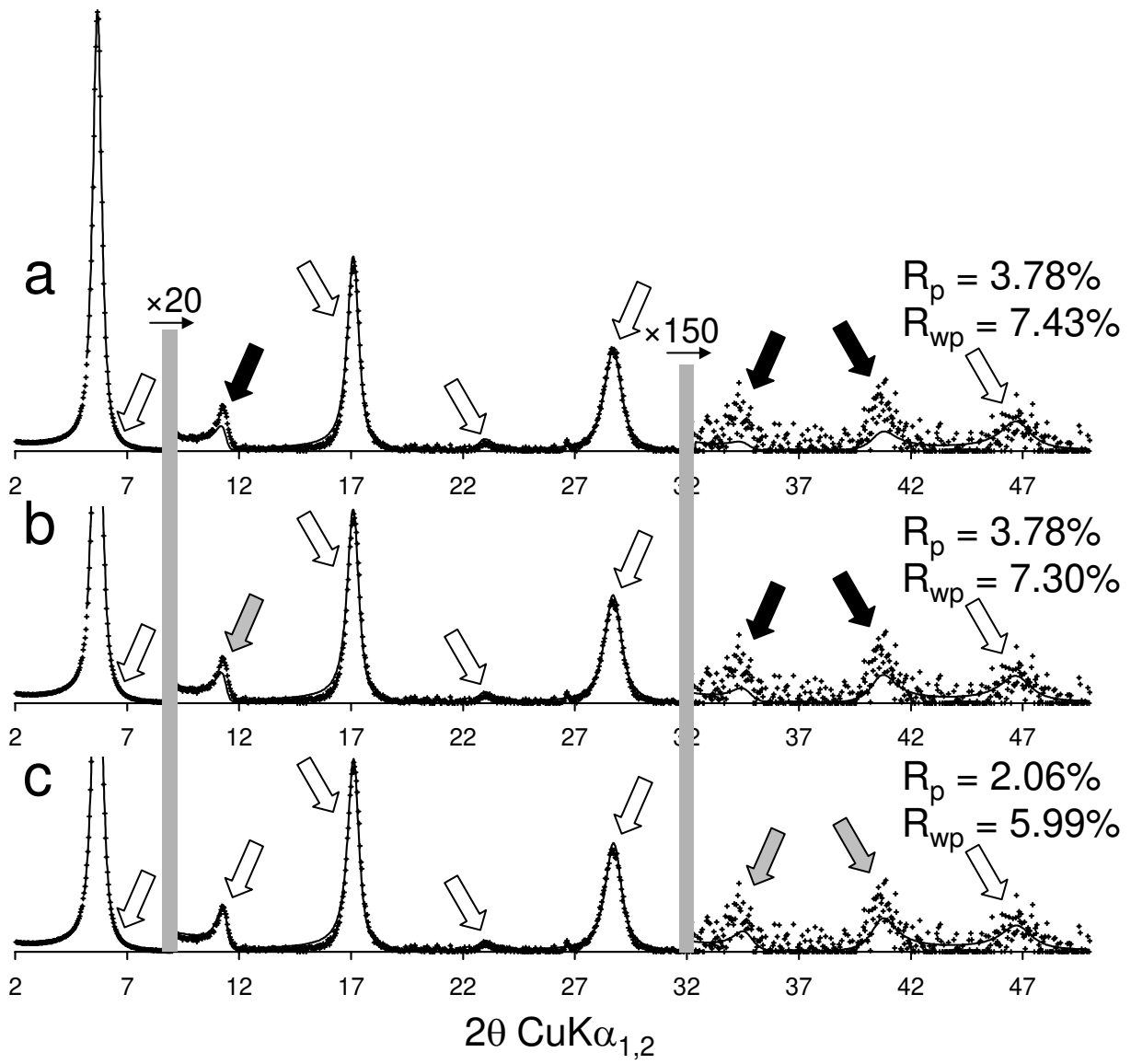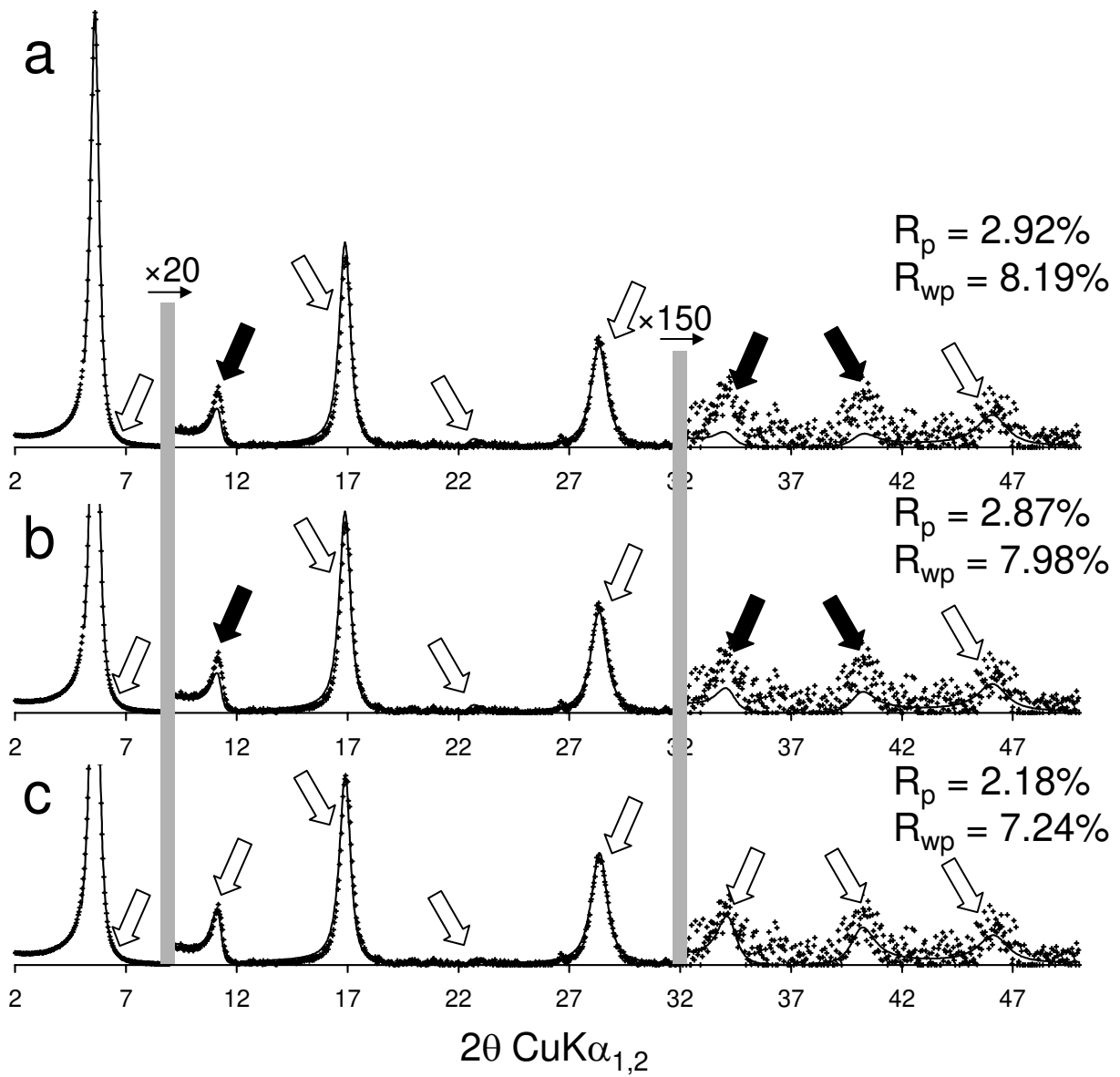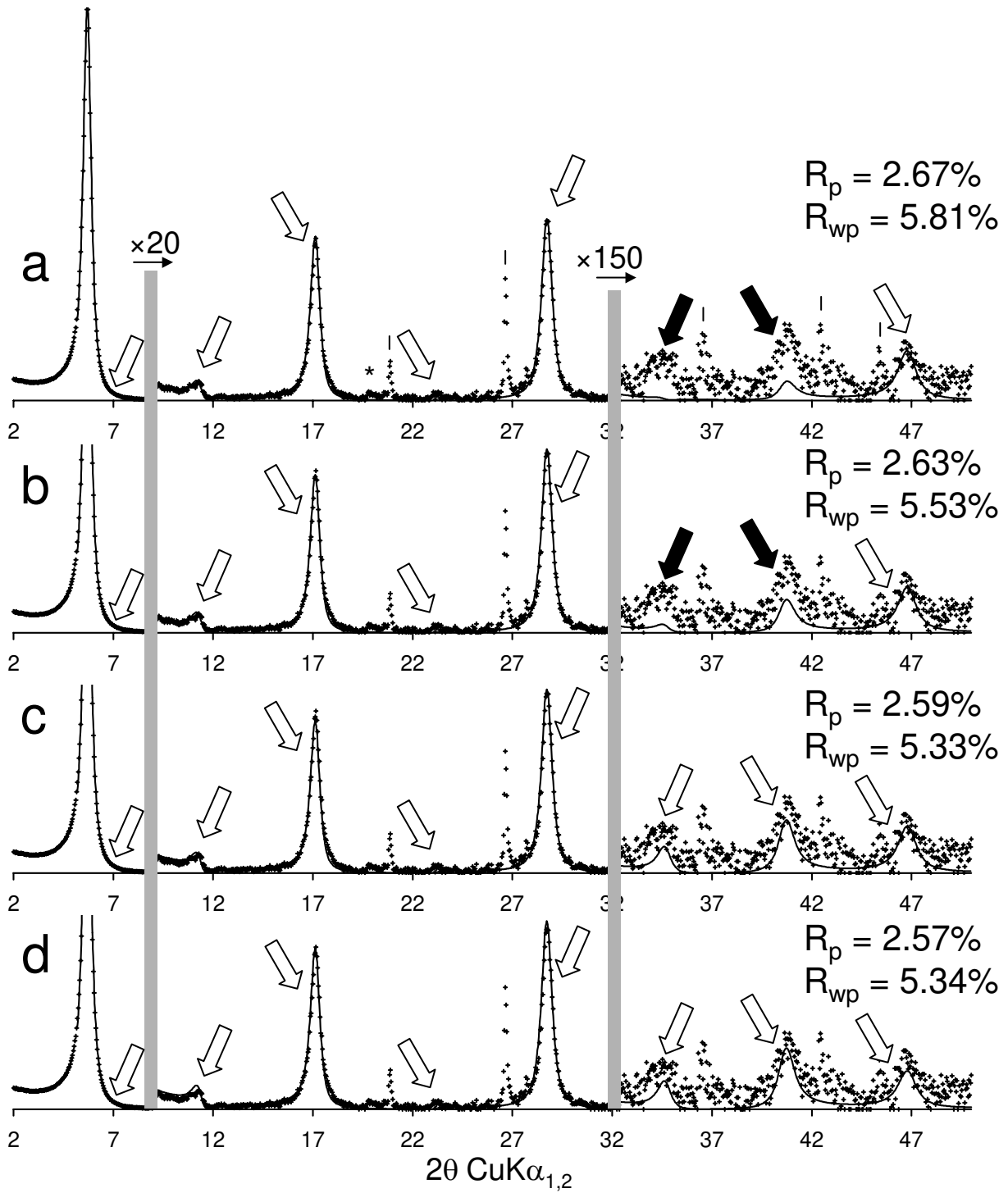
Ferrage et al. Fig. 01

Ferrage et al. Fig. 02

$R_p = 1.31\%$
$R_{wp} = 8.13\%$
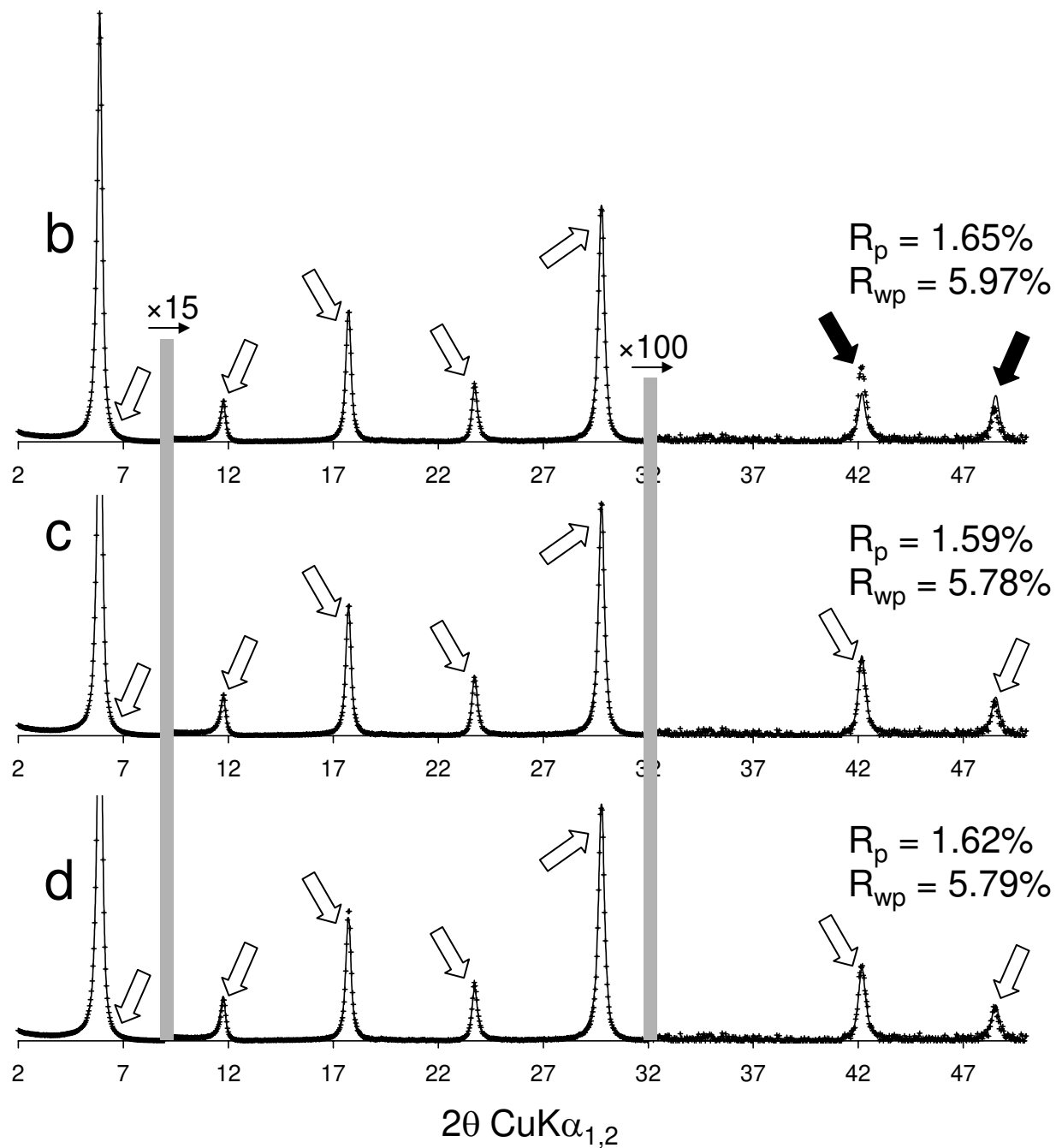
$R_p = 1.30\%$
$R_{wp} = 8.13\%$

$R_p = 1.28\%$
$R_{wp} = 8.02\%$

×20

×150

02,11

20,13

a

b

c

2θ CuKα$_{1,2}$

Ferrage et al. Fig. 03

a

×20

$R_p = 3.78\%$
$R_{wp} = 7.43\%$

×150

2 7 12 17 22 27 32 37 42 47

b

$R_p = 3.78\%$
$R_{wp} = 7.30\%$

2 7 12 17 22 27 32 37 42 47

c

$R_p = 2.06\%$
$R_{wp} = 5.99\%$

2 7 12 17 22 27 32 37 42 47

$2\theta\ CuK\alpha_{1,2}$

Ferrage et al. Fig. 04

a

$R_p = 2.92\%$
$R_{wp} = 8.19\%$

×20

×150

2   7   12   17   22   27   32   37   42   47

b

$R_p = 2.87\%$
$R_{wp} = 7.98\%$

2   7   12   17   22   27   32   37   42   47

c

$R_p = 2.18\%$
$R_{wp} = 7.24\%$

2   7   12   17   22   27   32   37   42   47

2θ CuK$\alpha_{1,2}$

Ferrage et al. Fig. 05

R_p = 2.67%
R_wp = 5.81%

R_p = 2.63%
R_wp = 5.53%

R_p = 2.59%
R_wp = 5.33%

R_p = 2.57%
R_wp = 5.34%

2θ CuK$\alpha_{1,2}$
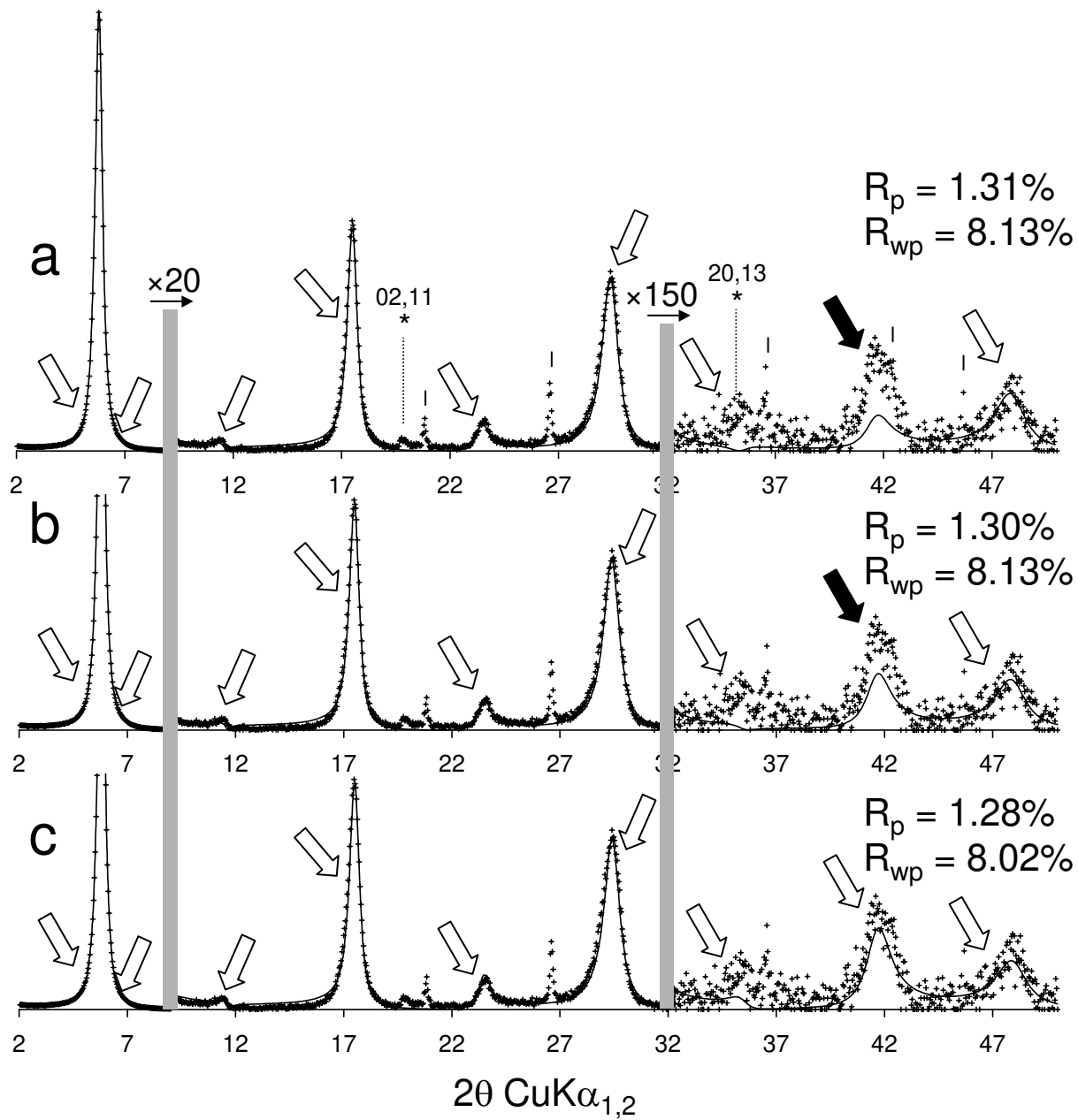
Ferrage et al. Fig. 06

Ferrage et al. Fig. 07

a

×8 →

×50 →

$R_p = 6.13\%$
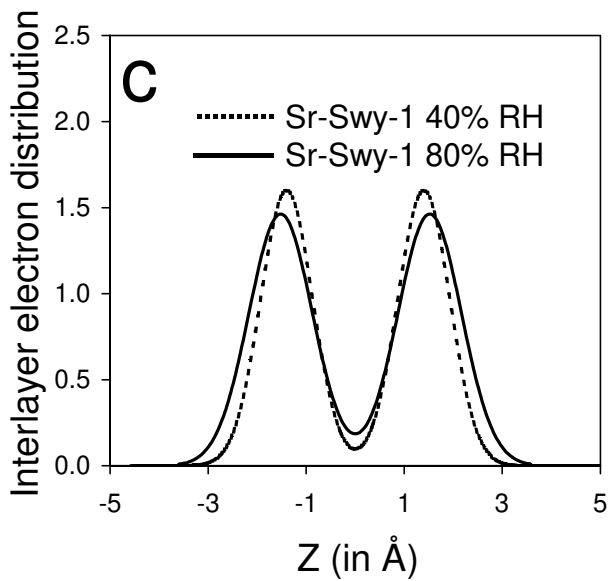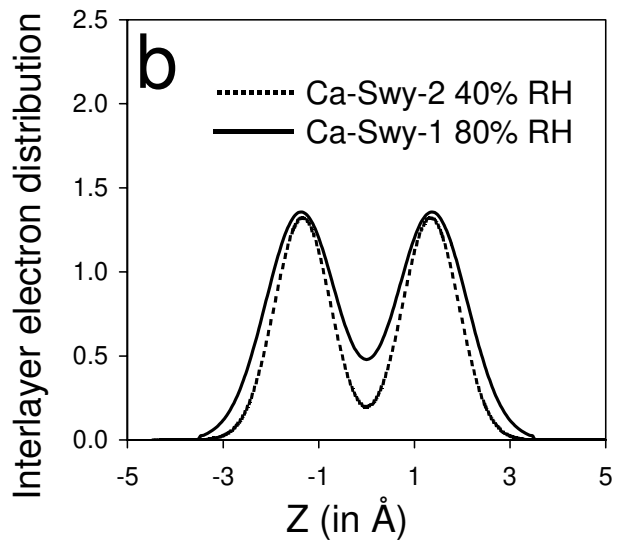$R_{wp} = 10.57\%$

b

$R_p = 6.14\%$
$R_{wp} = 9.79\%$

c

$R_p = 6.02\%$
$R_{wp} = 9.55\%$

d

$R_p = 6.14\%$
$R_{wp} = 9.73\%$

2   7   12   17   22   27   32   37   42   47

2θ CuK$\alpha_{1,2}$

Ferrage et al. Fig. 08

b

×15

×100

$R_p = 1.65\%$
$R_{wp} = 5.97\%$

2　7　12　17　22　27　32　37　42　47

c

$R_p = 1.59\%$
$R_{wp} = 5.78\%$

2　7　12　17　22　27　32　37　42　47

d

$R_p = 1.62\%$
$R_{wp} = 5.79\%$

2　7　12　17　22　27　32　37　42　47

2θ CuK$\alpha_{1,2}$

Ferrage et al. Fig. 09

a

$R_p = 2.76\%$
$R_{wp} = 12.00\%$

×20
×150

b

$R_p = 2.01\%$
$R_{wp} = 12.43\%$

×20
×150

02,11
*

20,13
*

c

$R_p = 4.30\%$
$R_{wp} = 12.94\%$

×20
×150

d

$R_p = 3.29\%$
$R_{wp} = 13.85\%$

×20
×150

e

$R_p = 3.23\%$
$R_{wp} = 11.30\%$

×20
×150

f

$R_p = 8.26\%$
$R_{wp} = 23.45\%$

×8
×50

g

$R_p = 3.14\%$
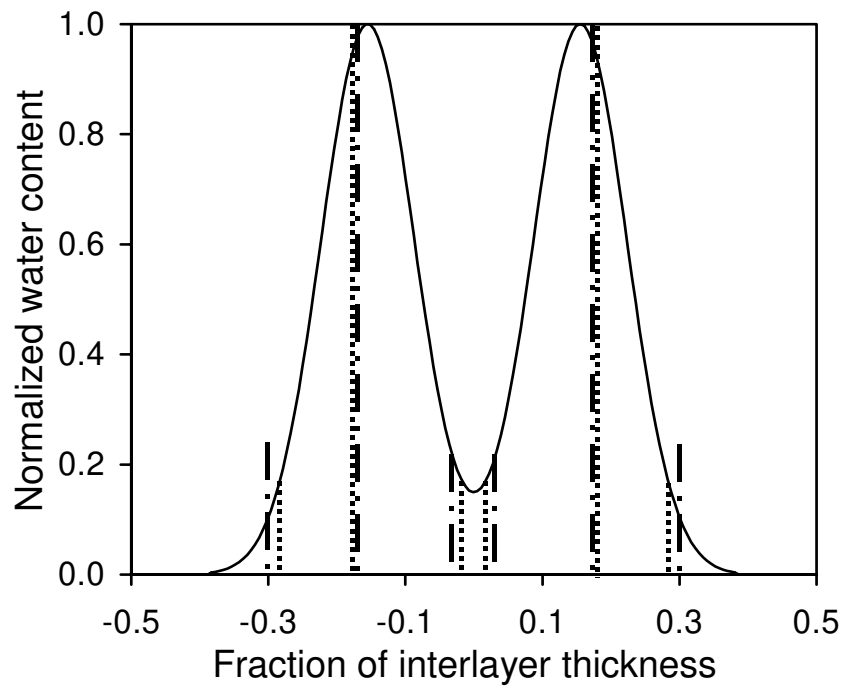$R_{wp} = 14.12\%$

×15
×50

2θ CuKα$_{1,2}$
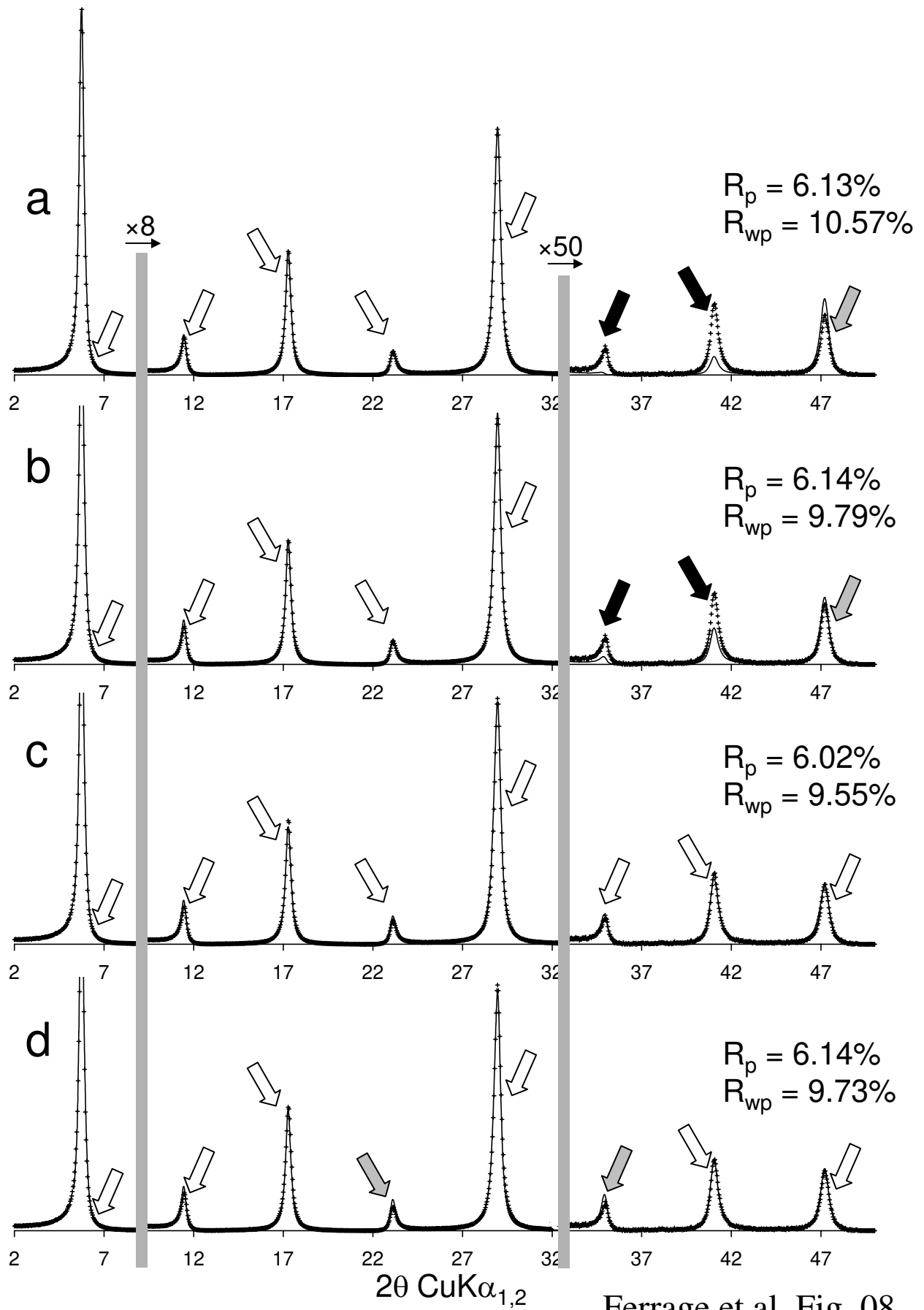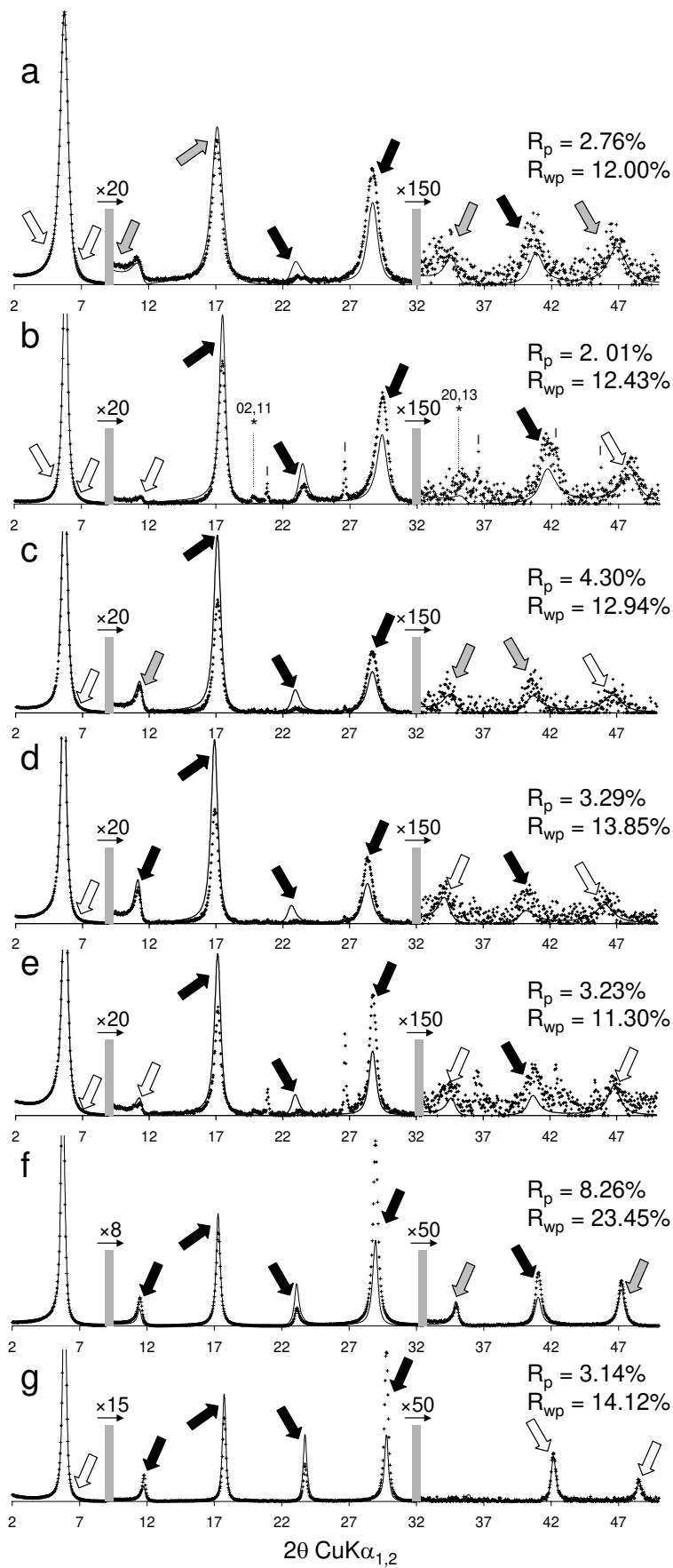
Ferrage et al. Fig. 10

Ferrage et al. Fig. 11

Type I   Type II

O
T

T
O

Type III   Type IV

O
T

T
O

Cat   H₂O

Ferrage et al. Fig. 12

Ferrage et al. Fig. 13

$R_p = 2.86\%$
$R_{wp} = 12.90\%$

$\times 15$

$\times 50$

$2\theta\ CuK\alpha_{1,2}$

Ferrage et al. Fig. 14